CENTRO DE INVESTIGACIONES EN ÓPTICA, A.C.

YTTERBIUM DOPED AND RAMAN FIBER LASERS

Thesis submitted in partial fulfillment of the requirements

for the degree of:

Doctor in Science (Optics)

M. C. Lelio de la Cruz May

October 2009, Leon Guanajuato.

Dedication

This work is dedicated to my wife Bartola and to my daughter Isabel.

Acknowledgments

First of all, I would like to thank my thesis director, Dr. Efrain Mejia Beltran, for his support and guidance in the elaboration of this thesis. Without his support I had not understood the rigors of scientific research.

I am indebted with the Ing. José Luís Orta Acuña and the Mtro. Andrés Salazar Dzib for their invaluable administrative support into Universidad Autónoma del Carmen (UNACAR) that allowed me to reach doctorate studies.

I would like to thank to CONACYT and PROMEP for their continuing support for my studying in the Centro de Investigaciones en Óptica.

Thanks also to all the research Staff and secretaries in the Centro de Investigaciones en Óptica.

Contents

Abstract

This thesis reports on theoretical and experimental results of a novel Raman fiber laser (RFL) consisting on the addition of an ytterbium-doped piece of fiber to the cavity. We investigated the level of enhancement of this approach in free-running and chained configurations. The addition of the doped-fiber notably decreased the laser threshold and increased the efficiency. We found that the amplified spontaneous emission produced by the doped fiber started the stimulated Raman scattering earlier than the spontaneous scattering in a 350-m silica-fiber cavity. In the best case, when splicing to the cavity 127 cm of doped fiber, the pump threshold decreased from 2.9 W down to 1.27 W, representing a 56% improvement. This power was close to the theoretical minimum of 1.25 W for very long fibers. The second stokes signal (1175 nm) was only present when the doped fibers were inserted. At 4-W pump, the non-doped cavity delivered 2 W of first stokes signal (1115 nm) that represent a 50 % efficiency compared to ~3 W delivered (~75 %) when a 34-cm doped fiber was inserted. This improvement is intended to reduce the cost of RFL's because less powerful sources or shorter fibers are necessary to produce more stokes components.

Introduction

Rare-Earth (RE) -ions are currently used to make optical fiber amplifiers and lasers capable of operating over a wide wavelength range from 0.4 to 4μm for applications in optical communications, spectroscopy, remote sensing, medicine instrumentations, material processing, frequency conversion, and more. The RE-doped fiber lasers (REDFL's) began its development in 1961 with the first demonstration of a Neodymium-doped fiber laser (NdDFL). This development was limited by the high attenuations in optical fibers and boomed in 1985 when the low-loss RE-doped optical fiber was a relatively mature technology and the laser diodes (LD's) delivering moderately high powers were available. By this time, special attention was on Nd- and Er-doped fiber lasers (ErDFL's), but other dopants such as holmium, samarium, thulium, and ytterbium appeared in the scene. Amplifiers and lasers with active optical fibers as the gain media have a remarkably superior performance over other schemes because of a high achievable gain, high efficiency, broad gain-linewidth, convenient heat-dissipation (due to the fiber structure), arguably temporal stability and compact size.

Within the family of RE- ions, ytterbium offers a broad spectral absorption and emission ranges, from ~800-nm to ~1064-nm for absorption and ~970-nm to ~1200-nm for emission. Two main absorption peaks at 915-nm and 976-nm are very close to the two main emission peaks at 975-nm and 1030-nm. This means that it is possible to have quantum efficiencies superior to 90%. Additionally, the broad emission spectrum above 1-μm makes ytterbium an attractive source for lasers and amplifiers. The Amplified Spontaneous Emission (ASE) saturates at very low powers in single mode fibers (about tens of milli-watts absorbed); it means that, after that pump power, they become practically transparent.

On the other hand, RFL's operate from the Spontaneous Raman scattering (SRS) produced by the molecular vibrations of the fiber material (usually non-RE-doped silica) when excited at high intensities because it is a non-linear effect. The 1064-nm pumped RFL's operate in the spectral region 1100-1700-nm that is attractive for applications in fiber optic communications, materials processing, signal processing, laser spectroscopy and medicine. The Raman gain depends mainly on the effective core area, fiber length, Raman cross sections, input pump intensity and Raman gain coefficient. To reach the Raman threshold in Raman fiber lasers it is necessary to apply high pump powers. However, in recent publications, the threshold has decreased due to the use of two types of optical fibers. In one of those, the core is doped with germanium (GeO_2-doped) and in the other with phosphorous (P_2O_5-doped). GeO_2-doped fiber possesses a rather broad Raman gain band (~100-cm^{-1}) with the peak at about 440-cm^{-1}. On the other hand, P_2O_5-doped fibers possess narrow band and the Raman peak at about 1330cm^{-1} (which is about three times larger than the frequency shift in GeO_2-doped fibers). In both fibers, refractive index modulations can be induced in the core by UV laser radiation. In this way, a periodic modulation in the core along some centimeters of fiber constitutes an interference filter called Bragg grating that usually works as a wavelength-selective mirror. A pair of Bragg gratings inscribed at both ends of an optical fiber may operate as an optical cavity. The Raman scattering (RS) is an adverse phenomenon in fiber-telecommunications because the information transmitted through a certain channel (at a specific wavelength) becomes present at other wavelengths that correspond to Stokes components and hence interferes with the information of the corresponding channels (cross-talk). Although the SRS signal is 10^{-6} times that of the pump power, when amplified over long distances it becomes seriously adverse. Conversely, the higher the RS, the higher efficiency of a FRL and as demonstrated in this work, if in addition an ASE signal from a doped fiber is present, the amplification process starts earlier, enhancing in this way the FRL performance.

Motivation

The main objective of this thesis is to investigate the behavior and characteristic of the power threshold for the Stokes generation inside a silica fiber in two configurations, when a fiber Bragg grating (FBG) is splicing to the silica fiber and when different pieces of 1000ppm Ytterbium-doped fiber laser (YbDF) are spliced between the FBG and the silica fiber in order to demonstrate that the ASE generated by the YbDF improves the power threshold.

Overview of the thesis

This thesis contains 3 chapters. The first chapter gives a general description of rare earth (RE)-doped fiber lasers based on reports of specialized literature; especially we put emphasis in the YbDF's. The second chapter describes the Raman scattering as well as the stimulated Raman Scattering in optical fibers, and the last chapter describes the experimental results, discussions and future trends.

Chapter I. Ytterbium Doped Fiber Lasers

I.1 Introduction

The first demonstration of laser action was reported on in 1960 and the active material was a ruby rod that emitted at 694-nm [1]. One year later, Snitzer demonstrated the first Nd^{3+}-doped silica fiber laser [2] emitting around 1060-nm in a multimode fiber. In 1962, Etzel, Grandy and Ginther observed and reported laser action in an ytterbium-doped silica fiber [3]. Nevertheless, at that time, Ytterbium doped Fiber lasers (YDFL's) were less attractive than Neodymium (NDFL's) because the generation in Nd^{3+} requires a four level pumping scheme, while Ytterbium (Yb^{3+}) is a quasi three level scheme for this wavelength. At that time fiber losses were extremely high, 1000dB/km compared to the modern standard of 0.2-dB/km in the 1.55μm wavelength region. In subsequent years more fiber lasers doped with other rare earths (RE's) were reported. However, rare-earth doped fiber lasers (REDFL) progressed slowly during twenty years due to the difficulties for manufacturing low–loss fiber and suitable pump sources. In fact, the major scientific study of fiber lasers boomed in 1985 with the development of a technique that incorporates RE in the core of an optical fiber during the fabrication of its preform. Such technique is termed modified chemical vapor deposition (MCVD) and makes use of vaporized halides or nitrates reacting with oxygen to form the required glasses [4],[5].

In recent years, REDFL's have experienced a rapid growth due to the fabrication and purification of fiber glasses, the development of laser diodes and optical components. Thanks to the development of high power InGaAs diodes emitting around 975-nm, YDFL's have turned out since early 1990s to be important competitors of NDFL's. At this time, Yb^{3+}-doped silica fibers present higher conversion efficiencies and output powers as well as a much broader emitting band that coincides with the line of Nd^{3+} [6]. The maximum

theoretical efficiency (quantum efficiency) is the energy that every photon generated takes from every pump photon and is given by their energy ratio that is the same as using the wavelength ratio. For Nd^{3+}, the efficiency is 76 % (808-nm/1064-nm ≈ 0.76) compared to 92 % (975-nm/1064-nm ≈ 0.92) for Yb^{3+}. This 16 % superiority in efficiency, together with the fact that the energy that is not optically extracted is converted to heat, makes the YbDFLs cooler than NdDFLs and then more capable of handling higher powers without requiring cooling systems. These laser sources are usually very robust and semi-compact because they mostly consist of an array of laser diodes that pumps an optical fiber that has mirrors attached to its ends and emits a circular beam that can be easily manipulated and focused to a small spot with ordinary optics. As a consequence, those lasers find applications in laser surgery, remote sensing, graphic arts, study of non-linear effects in optical fibers, materials processing, and so on.

I.2 Optical Fibers

A fiber laser is generally made of silica glass, although others types of glasses host have been investigated as fluoride and chalcogenide. In its simplest form, an optical fiber is a cylindrical dielectric waveguide that transports and guides energy in form of electromagnetic radiation. The optical fiber consists of a cylindrical core (with refractive index n_1) surrounded by a cylindrical cladding whose refractive index (n_2) is lower than that of the core; this difference produces total internal reflection (TIR) at the core-cladding interface and thus has the ability of confining light into the core. A protective polymer coating is employed to add strength and to prevent abrasion and physical damage caused by environmental exposure and handling during the installation process (see Figure 1).

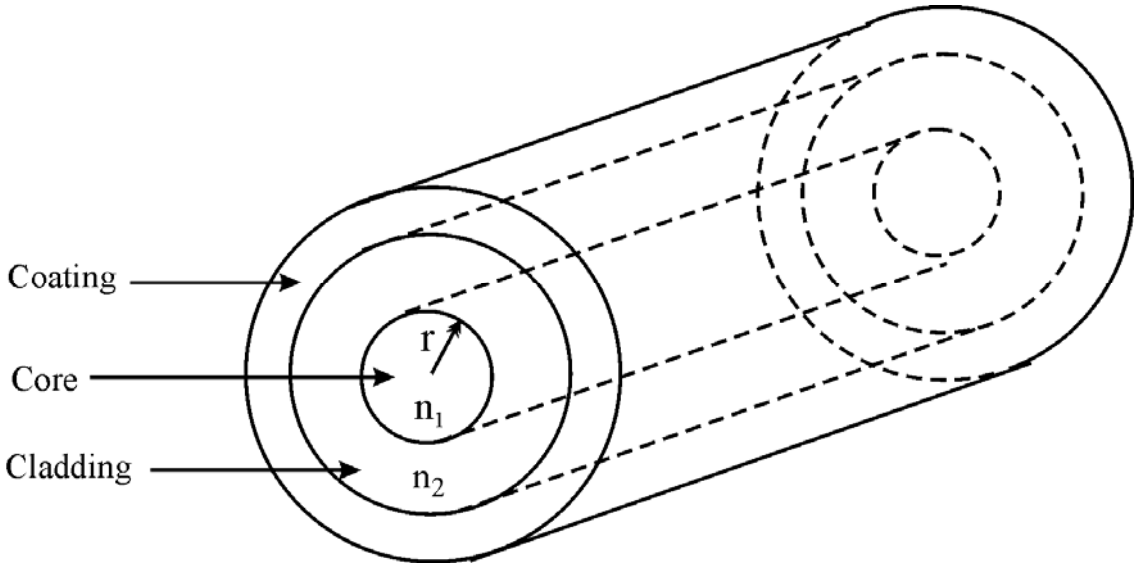

Figure 1. Optical fiber structure. The refractive indices of the core and cladding are n_1 and n_2 respectively, and $n_1>n_2$.

Two main categories of optical fibers are known as: a) Step-index fiber where both refractive indices are constant with an abrupt change at the core-cladding interface and $n_1>n_2$ and b) Graded-index fiber: where n_1 decreases gradually inside the core as a function of the radial distance r, i.e., $n_1(r)$ and n_2 remains constant.

The refractive index profile, the refractive index difference and the core diameter establish the confinement and propagation properties as well as the number of modes and the way they propagate along the fiber. Fibers that support many propagation transverse modes are called multi-mode fibers (MMF), while the fibers that support a single mode have smaller core diameters and are called single mode fibers (SMF). The most common type of SMF has a core diameter of 8-10μm, a cladding diameter of 125μm and is used for long distance communication; whereas the MMFs have typical core diameters of 50-μm to 60-μm and are mainly used for short distance. The cladding diameter of 125-μm and the total diameter 250-μm with the coating included are a standard in optical fibers.

When light propagates along an optical fiber its power (P_{in}) decreases exponentially with distance z. This attenuation is produced by scattering and material absorption. The output power is expressed as

$$P_{out}(z) = P_{in}\exp(-\alpha z) \tag{1}$$

Where α represents the loss coefficient and its units are m^{-1}. It is also conventional to express α in dB/km by using the relation

$$\alpha(\mathrm{dB/km}) = -\frac{10}{z}\log_{10}\left(\frac{P_{out}}{P_{in}}\right) \approx 4.343\alpha \tag{2}$$

The molecules of the glass give the minimum theoretical losses, being their size responsible of Rayleigh scattering that spreads the light in all directions with a maximum in the UV and a minimum at ~1600-nm. In addition, their vibrations have resonant bands that absorb in the infrared (IR) starting from a minimum value at ~1500-nm and keeping a moderate attenuation up to 2100-nm. Then, Rayleigh scattering establishes the higher energy transparency of silica glass at around 250-nm and the resonant vibration bands the low energy limit that practically makes it opaque beyond 2100-nm. The overlapping of these minimum-loss bands is at ~1500-1600-nm and it is the reason for the establishment of the telecommunication band in this region. Additional losses come from impurities not taken away during the glass preparation and as contamination or non-controlled physical defects during the fabrication of the fibers. The most important impurity affecting fiber loss is the OH ion, which has a fundamental vibrational absorption peak at 273-µm. The overtones of this OH-absorption peak are responsible for the dominant peak near 1.4-µm and a smaller peak near 1.23-µm.

As an example, a standard low-loss optical fiber typically used in fiber optic communication is the Corning SMF-28 and has 0.35 and 0.2dB/km loss at 1310-nm and 1550-nm, respectively.

RE-doped silica fibers are excellent materials for high-power lasers because they have a high optical damage threshold and their high surface/volume ratio makes heat dissipation very efficient. In a conventional single mode fiber laser pumped with a laser diode, the pump light is coupled into the core, this light added to the generated signal may reach the damage threshold. However, some Watts are supported in a single mode fiber laser. On the other hand, the output power of semiconductor lasers is limited by optical damage of their material. These two facts seriously affect diode-pumped fiber lasers. Besides, the efficiency with which the beam of a laser diode can be coupled into a fiber core is typically about 60% or less because of the non-circular shape of (moderately) high power laser diodes; hence, only a fraction of the available pump power is usable.

A commercial solution for real high-power laser diodes consists on arrays of multimode laser diodes that apart from consisting of multiple beams with different angles, in the best situation the overall shape is a square, but most times it is a rectangle. Coupling such a set of beams in a single mode core is a serious challenge. The best solution was invented by Snitzer and co-workers and consists of a single–mode RE-doped core surrounded by a first cladding with lower refractive index that is around 125-μm in diameter, this cladding is at the same time the core of a multimode optical fiber because it is surrounded by a second cladding (with still lower refractive index) that brings the total diameter beyond 200-μm in diameter (see Figure 2). This type of fiber is termed double clad fiber (DCF).

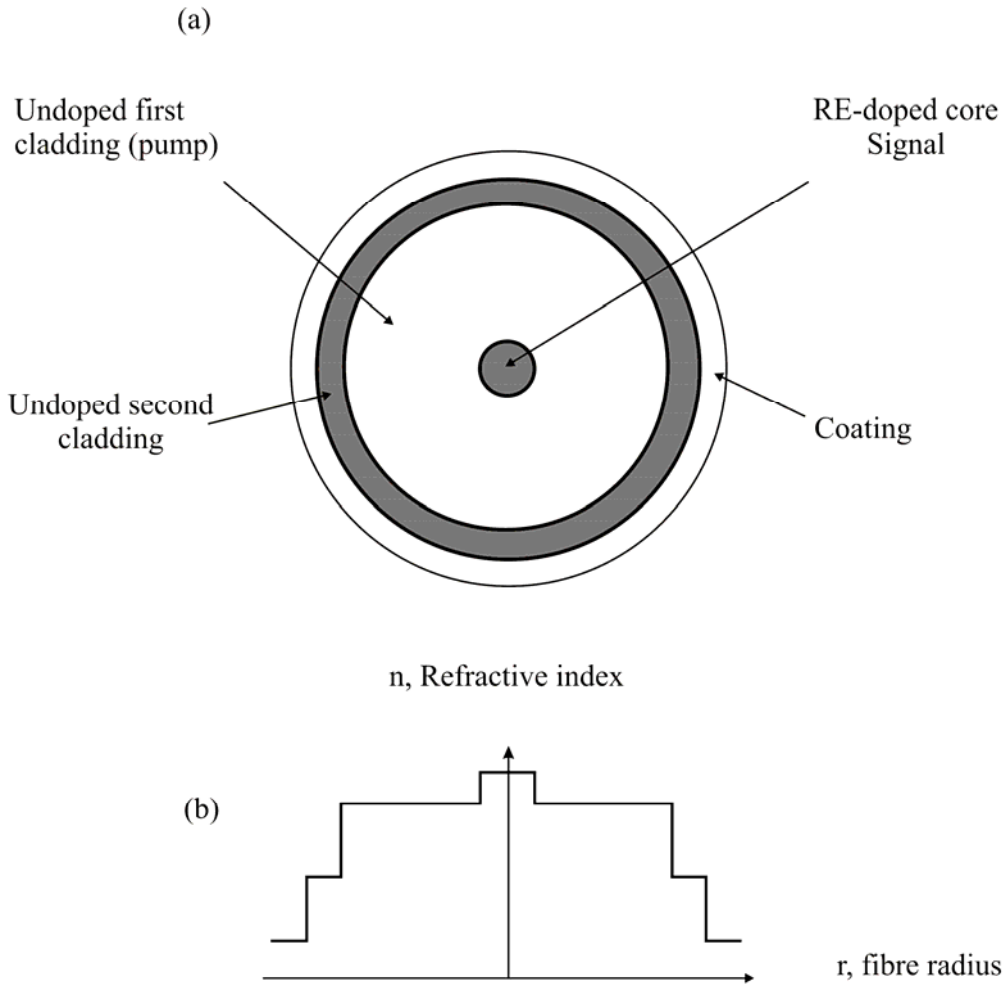

Figure 2. Double clad fiber: (a) basic configuration and (b) refractive index profile.

Now, the multimode part accepts the large structured spot produced by the array and as modes propagate, they encounter (several times) the single mode core that usually contains RE-ions that when excited, produce signal that becomes amplified. In this way, the highly-multimode pump is converted into a high-brightness single-mode signal. Nevertheless, within a double clad structure the pump-light absorption is significantly reduced compared to the conventional single–clad fibers. In order to improve the absorption, several geometries have been tested with good results. The idea has been basically to ensure that all the coupled rays eventually intercept the core, in particular the skew rays that travel along a spiral path. Various solutions are presented in Figure 3.

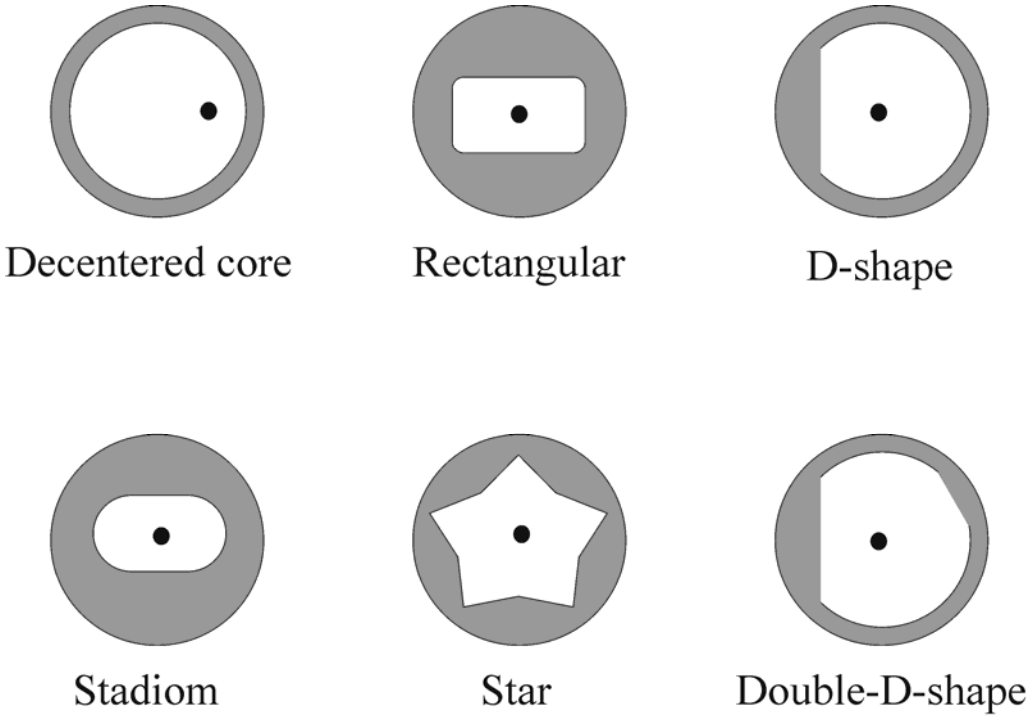

Figure 3. Applicable geometries of double clad for cladding pumping.

Thanks to the development of DCFs, the power of fiber lasers scaled up some orders of magnitude. For example, the 2-W Yb-doped fiber laser from 1995 [7], reached 35-W during 1997 [8], 110-W on 1999 [9], 610-W (2004) [10], and 2-kW on 2005 [11].

I.3 Three and four-level laser systems

The most important pumping schemes for fiber lasers depend on the energy level arrangement of the doped material and, in general, they can be classified as four or three–level systems (Figure 4). In real laser systems there may be many more levels involved in the action laser, but they can be simplified to either the four or three level system.

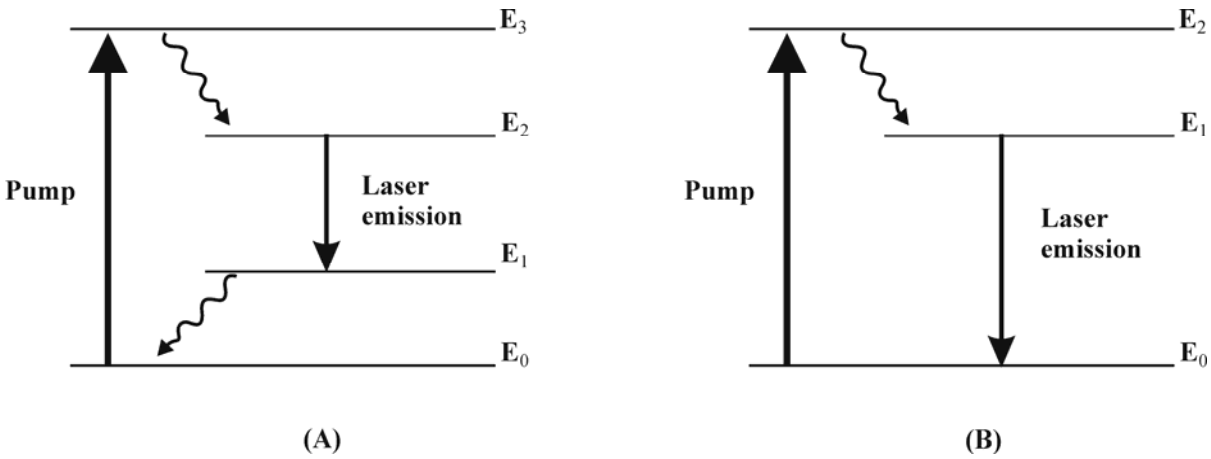

Figure 4. Simplified energy level structure of a four level laser (A) and three level laser (B).

Figure 4A shows the pumping scheme of a four-level laser. Without any excitation, all the RE^{3+}ions are in the ground level E_0. When exciting with the wavelength that corresponds to the energy difference between E_0 and E_3, the ions populate E_3 from where rapidly decay by releasing phonons down to E_2 where ion population accumulates because this level is metastable. Typical lifetime values in this level are from tens of microseconds to some milliseconds and depend on the type of glass that contains the dopants. The ratio between the populations that arrives to E_2 to the population that decays spontaneously after completing the lifetime is big. In addition, because the lifetime of the ions on E_1 (as on E_3) is quite short with typical values below some microseconds, those levels do not accumulate population and as a consequence it is possible to obtain population inversion between E_2 and E_1 ($N_2>>N_1$). Under this condition, spontaneously de-excitation of E_2 ions down to E_1 produces photons of energy E_2-E_1 that propagate mostly through excited ions. When a photon produced by spontaneous emission interacts with an excited ion, the later is forced to make a transition down to E_1 and two identical photons are generated that by interacting with two E_2 ions produce four and so on. This is the stimulated emission that gives rise to light amplification. Apart from being easy to achieve population inversion, if part of active material (doped fiber in this case) is not excited, no signal re-absorption occurs because the E_1-E_2 transition is inactive. Then, unlike three level systems, the optical fiber can be longer

than necessary without inducing losses other than those produced by the glass (usually negligible).

Figure 4B shows the three-level scheme. Here, the pumping transition is E_0-E_2 and fast nonradiative relaxations accumulate the population on E_1. Observe that the active transition here is E_1-E_0 and then, if part of fiber is not excited, signal re-absorption occurs because the high density of ions in the ground state (E_0) are excited to E_1. Then, unlike four level systems, three level systems present higher pump threshold because not only the entire fiber should be excited but all the fiber should be sufficiently excited to present population inversion; otherwise, considerable loss occurs and reaching the pump threshold for lasing becomes harder. Then, in these systems, there exists an optimal fiber length for each pump power level whereas in the four-level case, the fiber may exceed the required length. The advantages are: less fiber heating because there is only one step of non-radiative relaxation that implies material heating and as a consequence, higher theoretical efficiency.

I.4 Optical Transitions in Rare-Earth doped glasses

To understand why the RE-doped fibers (REDF's) amplify light signals, we first describe the electronic structure of the triply ionized state that the RE's acquire (RE^{3+}) when immersed as dopants in glasses. As such, the RE's change their energy by restructuring the 4f electronic structure when absorbing photons with the adequate energy (excitation) and after a short time return to their original electronic structure (de-excitation) called "ground state". This de-excitation produces one or more photons of lower energy than the excitation ones. All the discrete energies that a RE^{3+} may take are usually represented in an energy level diagram whose different levels are labeled in accordance to the vectorial contribution of the individual energies of all the electrons arranged accordingly.

The RE's are excellent elements to serve as active ions in solid-state laser materials because they exhibit absorption and emission bands throughout the UV-VIS-IR region of the electromagnetic spectrum. RE's are divided in two groups of 14 elements each, lanthanides and actinides. The lanthanides are characterized by the partially filled 4f sub-shell with atomic number 57 to 71. Their optical properties in the 3+-ionized state taken when doped in glasses makes them of great importance as active centers for lasers, in particular, for fiber lasers. The actinides are characterized by the partially-filled 5f sub-shell with atomic numbers 89 to 103 and because they are much less stable, their very short half-life makes them not useful for long lasting devices.

Electronic configuration of lanthanides have a common xenon (Z=54) in their electronic structures. In these atoms, the shells with quantum numbers n=1, 2, 3 are completely filled whereas the one with n=4 has its s, p, and d sub-shells filled and the 4f sub-shell that is capable of accommodating 14 electrons is empty. However, the n=5 shell has acquired its first 8 electrons filling the s and p-type orbits. Departing from Nd (Z=60), the 4f electrons contract so much that are protected from the environment by the outer 5s and 5p closed sub-shells. This shielding characteristic prevents the 4f electrons from interacting with the atom's environment and gives rise to relatively well defined absorption bands corresponding to excitation of the optically active 4f electrons. The electronic configuration of Xenon is

$$Xe=1s^2 2s^2 2p^6 3s^2 3p^6 3d^{10} 4s^2 4p^6 4d^{10} 5s^2 5p^6. \quad (3)$$

In the case of Yb (Z=70) in glass, the atom uses three electrons to form bonds to the glass and thus becomes triply ionized (Yb^{3+}) with the electronic structure that can be written as $Xe4f^{13}$.

Energy level structure of RE and other elements are expressed by capital letters of the form $^{2S+1}L_J$, where the orbital quantum numbers L=0, 1, 2, 3, 4, 5, are expressed by the capital letters S, P, D, F, G, H, I. (2S+1) indicates the multiplicity of the atomic energy

term due to possible orientation of the resultant spin S. J is the total angular momentum given by the combination of L and S. In a multi-electron atom there are several possible ways to obtain a given set of values for J, L, and S. Therefore, we refer to the coordinate of quantum states (J, L, and S) as a term. Each energy level is understood of 2J+1 quantum degenerate states (level multiplicity). For example, the notation $^2F_{7/2}$ for the ground state Yb^{3+}, corresponds to the term (7/2, 3, 1/2), which has a multiplicity L+1/2=7/2, and a spin multiplicity 2S+1=2. The energy levels are homogenously broadened by phonons interactions and are "Stark" split by perturbations of the local crystal field. The number of the Stark sub-levels in each energy level is given by the quantum state of the level and the host lattice. For example, for Yb3+ in silica glass, the $^2F_{5/2}$ level is split into 3 sub levels and $^2F_{7/2}$ ground is split into 4 sub-levels, giving a total of 12 Stark-level transitions around 1000-nm, see Figure 5.

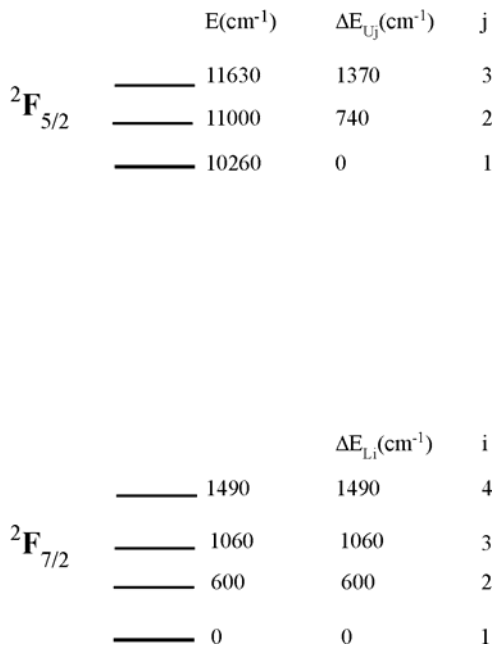

Figure 5. The Yb^{3+}-doped silica energy level structure, consisting of two manifolds, the ground manifold $^2\mathbf{F}_{7/2}$ with four Stark sublevels and excited manifold $^2\mathbf{F}_{5/2}$ with three Stark sublevels [7].

I.5 Yb^{3+}-doped Fiber Lasers.

In this section, we present the general theory behind the development of Yb^{3+}-doped fiber lasers that are the main topic of this work. Although no new material is presented here, we considered it important because some of the equations used in the next chapters are obtained here. Also described are some basic concepts that would occupy unnecessary space in the experimental report of this document.

I.5.1 Basic Configuration of a Fiber Laser

Although a variety of types of RE-doped lasers exists, all of them basically consist of three elements: a pumping source, an optical cavity that provides feedback and the active material, a RE-doped fiber (see Figure 6).

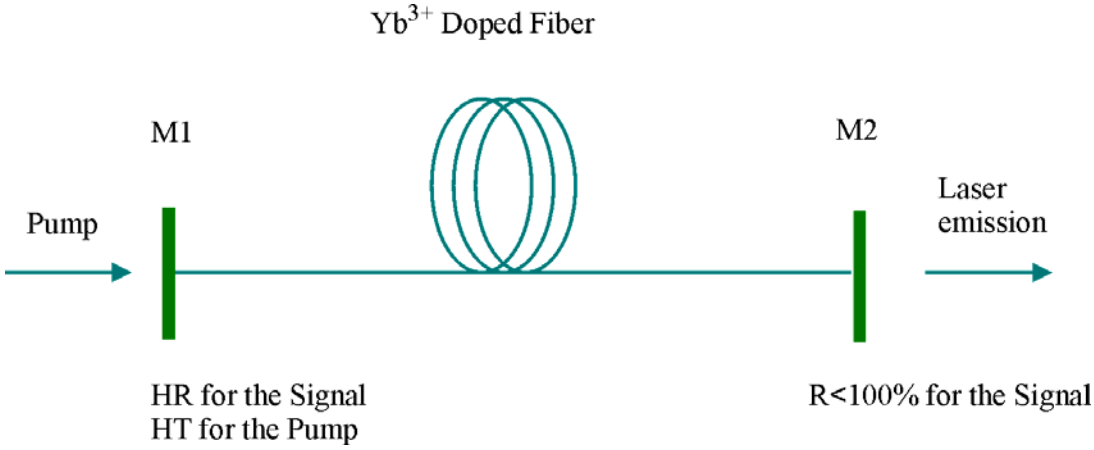

Figure 6. Typical configuration of a fiber laser. The mirror **M1** has high transmission (HT) for the pumped wavelength (λp) and high reflection (HR) for the laser emission wavelength (λs), and **M2** is partially transparent for the laser emission.

The pumping signal excites the atoms of the medium into a higher energy level to create population inversion that means amplification and therefore lasing. The pump is usually provided by another laser. In this work, the pump source was a diode-pumped fiber laser system operating at 1064-nm wavelength and the active material was an Yb^{3+}-doped optical fiber.

The optical cavity is created by two mirrors arranged such that the light amplifies as it travels back and forth through the gain medium. Usually one of the two mirrors (the output coupler) is partially transparent with the purpose that part of the signal is emitted through it. These mirrors can be dichroic filters, Bragg gratings or simply perpendicular cleaved facets of fiber-ends. In the later, highly efficient lasers only require the ~4% of the amplified signal to travel back into the cavity to be re-amplified and the rest (96%) is delivered as useful laser light.

I.5.2 Spectroscopy of Yb^{3+}

Ytterbium is one of the most versatile ions for lasing at around 1000-nm in silica [7] given that its spectrum exhibits unusual broad absorption and emission bands from ~800-nm to ~1064-nm for absorption and ~970-nm to ~1200-nm for emission in the $^2\mathbf{F}_{7/2} \rightarrow {}^2\mathbf{F}_{5/2}$ transition (See Figure 7). The absorption and emission spectra depend to some extent on the host glass composition [12] but most of them look like the spectra shown in Figure 7 [13]. Due to the broad absorption band the Yb^{3+} doped silica fiber can be pumped with a wide selection of diode lasers such as AlGaAs (~800-850-nm) and InGaAs (980-nm) or solid-state lasers such as Nd:YLF (1047-nm) and Nd:YAG (1064-nm). Observe that the fluorescence is broader than the one from NdDFL's, this makes Yb^{3+} more attractive than Nd^{3+} because a broader wavelength range is available for oscillation.

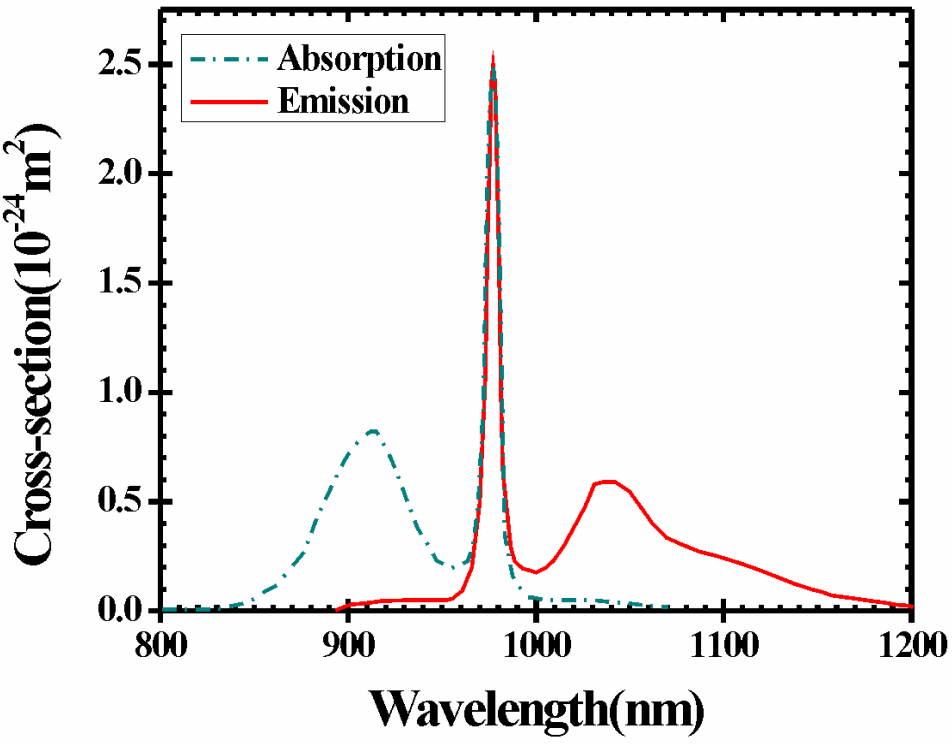

Figure 7. Absorption and emission cross sections of Ytterbium. The fiber core was doped with 550±100ppm in germanosilicate host [7].

The ytterbium has quite a simple energy level arrangement as one may observe in Figure 5. It has only the ground state $^2\mathbf{F}_{7/2}$ (with four Stark levels) and a metastable state $^2\mathbf{F}_{5/2}$ (with three Stark sublevels) spaced by approximately 10,000-cm^{-1} [7]. The Ytterbium ions hosted in glass present the absorption and emission spectra that correspond to the overlapping of the in-homogeneously broadened Stark sublevels, because contrary to crystals where all the ions have the same spectra because of interactions with the same crystal field (homogeneous broadening), in glasses, each ion is subjected to a different glass field because the matrix consists of distorted crystal cells. For this reason, each ion has its own spectroscopic characteristics. YbDFLs are typically pumped into the higher sublevels of the $^2\mathbf{F}_{5/2}$ manifold; at emission wavelengths below 990-nm they behave as a three–level system, whereas at longer wavelength, from ~1000 to 1200-nm, the system is quasi-four-level. The radiative lifetime of the $^2\mathbf{F}_{5/2}$ state is typically in the range of 700-1400-μs,

depending on the host and the absence of higher energy levels greatly reduces the multi-phonon relaxations and the possibility of having signal re-absorption by excited ions i.e. “excited state absorption” or ESA. The absence of overheat, together with no signal-wasting makes the scheme capable of producing high power. Yet another benefit is the abnormally high absorption and emission cross sections that are typically several times higher than in multi-component glasses. These combined features allow for very strong pump absorption and very short fiber lasers [14].

I.5.3 Population Dynamics and Propagation Equations

In this section, an idealized model of a three level laser is used to understand the population dynamics and propagation equations of the pump and the signal throughout an ytterbium doped fiber. Figure 8 shows the corresponding energy level diagram, where level 1 is the ground level, level 2 is the metastable level characterized by a long lifetime τ and level 3 is the pump level.

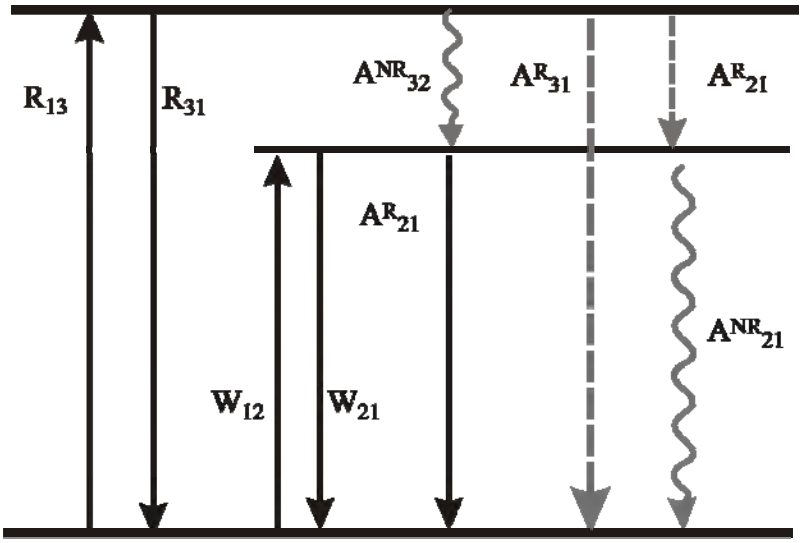

Figure 8. Simplified energy level diagram of a three-level laser, where R, W, and A correspond to pumping rates, stimulated emission rates, and spontaneous decay rates

between related levels; superscripts R and NR refer to radiative and nonradiative emission rates, respectively[15].

R_{13} is the pumping rate from levels 1 and 3, and R_{31} is the stimulated emission rate between level 3 and 1. Two possibilities of decay occur from the excited state corresponding to level 3, radiative (rate $A^R_3 = A^R_{32} + A^R_{31}$) and nonradiative (rate A^{NR}_{32}). W_{12} and W_{21} are the stimulated absorption and emission rates between levels 1 and 2, respectively. The spontaneous radiative and nonradiative decay from the excited state corresponding to level 2 is $A_2 = A^R_{21} + A^{NR}_{21}$ with $A^R_{21} = 1/\tau$, τ is fluorescence lifetime. It is assumed that the spontaneous decay is essentially radiative, i.e., $A^R_{21} >> A^{NR}_{21}$. The total population of the levels 1, 2 and 3 are designed N_1, N_2, and N_3, respectively. The total population N is then $N = N_1 + N_2 + N_3$. The atomic rate equations corresponding to these populations are [15]:

$$\frac{dN_1}{dt} = -R_{13}N_1 + R_{31}N_3 - W_{12}N_1 + W_{21}N_2 + A_{21}N_2 \tag{4}$$

$$\frac{dN_2}{dt} = W_{12}N_1 - W_{21}N_2 - A_{21}N_2 + A_{32}N_3 \tag{5}$$

$$\frac{dN_3}{dt} = R_{13}N_1 - R_{31}N_3 - A_{32}N_3 \tag{6}$$

If the excited level is very near the metastable level then the transitions from level 3 to level 2 are instantaneous in such a way that in all moment the population in the level 3 is approximately zero, i.e., $N_3 \approx 0$. This reasoning implies that $A_{32}N_3 = R_{13}N_1 - R_{31}N_3$. Based on this supposition the equation 5 is re-written as:

$$\frac{dN_2}{dt} = W_{12}N_1 - W_{21}N_2 - A_{21}N_2 + R_{13}N_1 - R_{31}N_3 \tag{7}$$

The previous argument supposes that the transitions ideally are happening between the levels 1 and 2, therefore we should change the order of the transitions sub-indexes, i.e. R_{13} to change for R_{12} and $R_{31}N_3$ to change for $R_{21}N_2$. Performing these changes in the equations 1 and 2 we obtain the equations that model the behavior of an Yb^{3+}-doped fiber laser given by:

$$\frac{dN_2}{dt} = (R_{12} + W_{12})N_1 - (R_{21} + W_{21} + A_{21})N_2 \tag{8}$$

$$\frac{dN_1}{dt} = -(R_{12} + W_{12})N_1 + (R_{21} + W_{21} + A_{21})N_2 \tag{9}$$

If we consider now the steady state regime where the populations are time invariant, i.e., $dN_i/dt=0$ and solving for N_2 and N_1 we obtain,

$$N_2 = \frac{R_{12} + W_{12}}{R_{12} + R_{21} + W_{12} + W_{21} + A_{21}} N \tag{10}$$

$$N_1 = N - N_2 \tag{11}$$

These transitions rates are related with well-known parameters as the absorption and emission cross section, and pumping and signal intensities as;

$$R_{12} = \sigma_a^p I_p / h\nu_p, \; R_{21} = \sigma_e^p I_p / h\nu_p \tag{12}$$

$$W_{12} = \sigma_a^s I_S / h\nu_S, W_{21} = \sigma_e^s I_s / h\nu_s, \; A_{21} = 1/\tau \tag{13}$$

Where σ_a^p and σ_e^p are the effective pump absorption and emission cross sections, σ_a^s and σ_e^s are corresponding values for the signal absorption and emission cross sections, τ is the time of spontaneous emission from level 2 to level 1, and I_p and I_s are the pump and signal intensities (in W/m^2).

The population in the excited and fundamentals levels can be expressed in function of experimental values, by using next transformations $I_p=P_p/A_{inner}$ and $I_s=P_s/A_{core}$, then the eq. (10) is rewritten as:

$$N_2 = \frac{\frac{\sigma_a^p P_p}{A_{inner} h\nu_p} + \frac{\sigma_a^s P_s}{A_{core} h\nu_s}}{\frac{\sigma_a^p P_p}{A_{inner} h\nu_p} + \frac{\sigma_a^s P_s}{A_{core} h\nu_s} + \frac{\sigma_e^p P_p}{A_{inner} h\nu_p} + \frac{\sigma_e^s P_s}{A_{core} h\nu_s} + \frac{1}{\tau}} N \tag{14}$$

Associating common terms the expression becomes:

$$N_2 = \frac{\frac{\sigma_a^p P_p}{A_{inner} h\nu_p}\tau + \frac{\sigma_a^s P_s}{A_{core} h\nu_s}\tau}{P_p\left(\frac{\sigma_a^p + \sigma_e^p}{A_{inner} h\nu_p}\right)\tau + P_s\left(\frac{\sigma_a^s + \sigma_e^s}{A_{core} h\nu_s}\right)\tau + 1} N \tag{15}$$

The expressions $\frac{A_{inner} h\nu_p}{(\sigma_a^p + \sigma_e^p)\tau}$ and $\frac{A_{core} h\nu_s}{(\sigma_a^s + \sigma_e^s)\tau}$ are defined by Paschotta et. al. [13] such as P_{psat} and P_{ssat} pump saturation power and saturation signal, respectively. The pump saturation power is the power which reduces the absorption coefficient by a factor of two. A_{core} and A_{inner} are areas of the core and inner cladding respectively.

Substituting these new expressions, finally a mathematical expression is obtained for the population in the excited state in function of the input power and output signal given by

$$N_2 = \frac{\frac{P_p}{(\sigma_e^s/\sigma_a^s + 1)P_{psat}} + \frac{P_s}{(\sigma_e^p/\sigma_a^p + 1)P_{ssat}}}{\frac{P_p}{P_{psat}} + \frac{P_s}{P_{ssat}} + 1} N \tag{16}$$

In this way, the gain for the signal and loss for pump at any point along the fiber z is given by:

$$\frac{dP_s^{\pm}(z)}{dz} = \pm\Gamma_s[\sigma_e^s N_2(z) - \sigma_a^s N_1(z)]P_s^{\pm}(z) \quad (17)$$

$$\frac{dP_p(z)}{dz} = \Gamma_p[\sigma_e^p N_2(z) - \sigma_a^p N_1(z)]P_p(z) \quad (18)$$

Where $\Gamma_{p,s}$ represent the overlapping factor for the pump and signal for a Yb^{3+} double clad fiber, respectively. For the usual single-mode fibers, reasonable accuracy is achieved with the approximation of constant pump and signal intensities over the cross section of the fiber core if additional overlap factors Γ_p and Γ_s are introduced to account for the fact that some fraction of the power propagates in the un-doped cladding of the fiber.

I.5.4 Amplification and gain coefficients

In the previous section, we expressed rate equations for both pump and signal. These equations are related with the atomic populations N_1 and N_2, which were written explicitly in terms of pump and signal powers. To quantify a relationship for the gain of a laser, we may consider first the induced transition rate W_{21} between two energy levels of an ion as

$$W_{21} = B_{21}\rho(\nu) \quad (19)$$

Where $\rho(\nu)$ is the energy density (J/m^3) of the electromagnetic field inducing the transition, and B_{21} is the stimulated emission parameter of the level 2 to level 1 transition given by

$$B_{21} = \frac{c^3}{8\pi n^3 h\nu^3} A_{21} \tag{20}$$

$A_{21}=1/\tau$, n is the material refractive index, h Boltzmann's constant and c is the speed of the light in vacuum. In a similar way, the induced transition rate from level 1 to level 2 (absorption) is given by

$$W_{12} = B_{12}\rho(\nu) \tag{22}$$

Another way for expressing equation (19) is:

$$W_{21} = \frac{c^3\rho(\nu)}{8\pi n^3 h\nu^3 \tau} \tag{23}$$

In the case where the inducing radiation is monochromatic at frequencyν, then the induced transition rate from level 2 to level 1 is

$$W_{21} = \frac{c^3\rho_\nu g(\nu)}{8\pi n^3 h\nu^3 \tau} \tag{24}$$

Where $g(\nu)$ is the transition lineshape function, normalized such that

$$\int_{-\infty}^{\infty} g(\nu)d\nu = 1 \tag{25}$$

$g(\nu)d\nu$ is the probability that a particular stimulated emission event from level 2 to level 1 will result in a photon with a frequency between ν and $\nu+d\nu$. On the other hand, the inducing field intensity (W/m^2) is

$$I_\nu = \frac{c}{n}\rho_\nu \tag{26}$$

Then, the induced transition rate W_{21} becomes

$$W_{21} = \frac{c^2 g(\nu) I_\nu}{8\pi n^2 h\nu^3 \tau} \tag{27}$$

Eq. 27 gives the relationship between the stimulated transition rate in a laser medium and the optical field intensity. In the specific case of a monochromatic plane wave propagating in the z-direction through a gain medium with cross –section area A and elemental length dz, the net power dP_ν generated by a volume Adz of the medium is the difference in the induced transition rates between the levels multiplied by the transition energy $h\nu$ and the elemental volume as:

$$\begin{aligned} dP_\nu &= \left(\left[\frac{c^2}{8\pi n^2 h\nu^3 \tau} g_e(\nu)\right] N_2 - \left[\frac{c^2}{8\pi n^2 h\nu^3 \tau} g_a(\nu)\right] N_1\right) I_\nu h\nu A dz \\ &= (\sigma_e^s N_2 - \sigma_a^s N_1) P_\nu dz \\ &= g_m(\nu) P_\nu \end{aligned} \tag{28}$$

Where $g_e(\nu)$ and $g_a(\nu)$ are the emission and absorption line shapes, respectively. The terms inside the brackets in the Eq. 28 are the emission and absorption cross sections, and $g_m(\nu)$ is the local gain coefficient. Eq. 28 implies that to achieve positive gain a population inversion must exist between level 2 and level 1. Therefore, the gain measures the strength of optical amplification (the ratio of output power and input power) and is function of

population densities in different electronic levels. The gain in a length L can be expressed by

$$G = \int_0^L [\sigma_e^s N_2(z) - \sigma_a^s N_1(z)]dz \tag{29}$$

Using the Eqs. (17), (18) and assuming that the pump and laser intensities are not uniform over the core area, which is normally the case for the cladding pumping fiber laser, the gain can be expressed by

$$G = \frac{\Gamma_s}{\Gamma_p}\frac{(\sigma_e^s + \sigma_a^s)}{(\sigma_e^p + \sigma_a^p)}\left[\ln\left(\frac{P_p(L)}{P_p(0)}\right) + \Gamma_p \sigma_a^p NL\right] - \Gamma_s \sigma_a^s NL \tag{30}$$

Where $P_p(0)$ and $P_p(L)$ represents the input power and output pump power, respectively, and L is the fiber length of Yb^{3+}-doped double clad fiber. Γ_s Is the overlap factor of laser mode field with the doped area, $\Gamma_p = S_d / S_{ic}$ is the overlap factor of pump mode field with the doped area, S_d and S_{ic} are the core and inner cladding cross section of Yb^{3+} -doped double clad fiber. Parameters of the gain are known values except the emission and absorption cross section for the signal, which depends on the frequency throughout the emission bandwidth; this implies that the gain extends through the bandwidth for any fiber length.

I.5.5 Absorption and emission cross sections

The performance of any Yb^{3+}-doped glass laser may be valued from the emission and absorption properties. Absorption and emission cross section are the probability for absorbing or emitting a photon to induce a transition in the medium from ground state to

excited estate or excited state to ground state. Cross sections allow treating the laser medium as a two-level system. These are determined using either the method of reciprocity (MR) better known as McCumber Analysis or the Fuchtbauer-Ladenburg (F-L) formula. The cross section described by reciprocity method requires absolute polarized absorption cross section and detailed knowledge of the energy levels and degeneracy. While to determine the cross section for F-L formula need input parameter with the emission line shape function, the radiative lifetime and the refractive index.

McCumber Analysis supposes that the emission cross section $\sigma_e(\lambda)$ can be well calculated from the measured absorption cross section $\sigma_a(\lambda)$ as:

$$\sigma_e(\lambda) = \sigma_a(\lambda)\frac{Z_L}{Z_u}\exp\left[\frac{E_{UL} - hc/\lambda}{k_B T}\right] \tag{31}$$

Where Z_L, Z_U represent the partition functions of the lower and the upper states, respectively, given by:

$$Z_L = \sum_i \exp\left(-\frac{\Delta E_{Li}}{k_B T}\right) \tag{32}$$

$$Z_U = \sum_j \exp\left(-\frac{\Delta E_{Uj}}{k_B T}\right) \tag{33}$$

Where T is the absolute temperature in Kelvin, E_{UL} is the energy difference between the lowest sub-levels in the upper and lower manifolds (see Figure 5), and ΔE_{Uj} and ΔE_{Li} are energy levels in the upper manifold and lower manifold, respectively [16]. McCumber analysis may be employed for those materials with detailed energy level data.

The Fuchtbauer-Ladenburg (F-L) formula involves the fundamental relationship between spontaneous and stimulated emission rates. The form of the equation of cross section emission and absorption are

$$\sigma_e(\lambda) = \frac{\lambda^4 A_{rad}}{8\pi c n^2} g(\lambda) \tag{34}$$

Where $g(\lambda)$ is referred to the normalized line shape function of the $^2F_{5/2} \rightarrow {}^2F_{7/2}$ transition of Yb^{3+} and A_{rad} is the spontaneous emission probability which can be calculated from

$$A_{rad} = \frac{8\pi c n^2 (2J'+1)}{\lambda_p^4 N(2J+1)} \int \alpha(\lambda) d\lambda \tag{35}$$

Where J and J' are the total momentums for the upper and lower levels, $\alpha(\lambda)$ is the absorption coefficient, and λ_p is the absorption peak wavelength.

I.5.6 Amplified Spontaneous Emission (ASE)

An atom in an excited state will spontaneously decay to a state of lower energy after τ, releasing energy in the form of a photon, which is emitted in a random direction. This process is called spontaneous emission. It is also possible that the emission is stimulated by incoming photons, in which case the process is called stimulated emission. A spontaneous photon does not have coherence with any other. Therefore the collection of such spontaneously generated photons forms a background noise added to any signal intentionally generated. This background noise is called amplified spontaneous emission (ASE).

An analysis of Desurvire [15] shows that the number of randomly photons at frequency between ν and ν+δν that are spontaneously generated in the direction of positive z, within an infinitesimal volume dV of a laser medium, and coupled into the fiber mode, are given by:

$$dn(\nu) = A_{21} g(\nu) \delta\nu \frac{\Delta\Omega}{4\pi} dV \int_s N_2(r,\theta) \overline{\psi}_s(r,\theta) r dr d\theta \tag{36}$$

Where $\Delta\Omega/4\pi$ is the factor the spontaneous light captured by the fiber core, and the integral term accounts for the overlap between the density distribution of excited ions and the guided mode. And then, the rate of creation of spontaneous emission power in bandwidth $\delta\nu$ becomes:

$$\frac{dP_{ASE}}{dz} = 2P_0 \sigma_e(\nu) \int_s N_2(r,\theta) \overline{\psi}_s(r,\theta) r dr d\theta \tag{37}$$

Where $P_0 = h\nu\delta\nu$ is the power of one spontaneous noise photon in the bandwidth $\delta\nu$. The term P_0 is often referred to as an equivalent input noise because in high gain conditions the total spontaneous emission generated along the fiber is equivalent to the amplification of one fictitious input photon per mode within $\delta\nu$. The factor 2 in the Eq. (37) reflects that the spontaneous emission occurs in both polarization modes of the fiber.

With the rate of creation of spontaneous emission power at z and propagating in the positive direction, the evolution of the total signal at λ_s within $\delta\nu$ is expressed by:

$$\frac{dP_s(\lambda_s)}{dz} = \sigma_a(\lambda_s) 2\pi \int_s \{\eta(\lambda_s) N_2(r)[P_s(\lambda_s) + 2P_0] - N_1(r) P_s(\lambda_s)\} \overline{\psi}(r) r dr \tag{38}$$

The above equation describes phenomena, signal and noise amplification. If N_2 is different from zero, the constant term $2P_0$ in the right-hand side of the equation causes the

generation of optical noise along the fiber, whether optical signal was or not coupled to the fiber, which represents the total guided ASE in $\delta\nu$. ASE is also generated and propagated in the direction opposite to z.

I.6 Conclusions

In this chapter a general discussion of the RE-doped fiber lasers is described, especially it is emphasized in the YbDFL's. Due to the simplicity of the level structure of the Yb-ion others scheme of pumping are analyzed with the purpose of obtaining high power fiber lasers. A mathematical expression is also obtained to describe signal gain and loss for the pump at any point z a long the fiber.

We also analyzed the absorption and emission cross section calculation for ytterbium ions useful for simulations of the pumping and laser signal propagation. Finally, gain and ASE were discussed as important parameters that determine the performance of the rare earth fiber laser.

References

[1] Mainman, T. H., “Optical and microwave optical experiments in Ruby”, Phys. Rev. Lett., 4, pp. 564 (1960)

[2] Snitzer, E., “Optical maser action in Nd3+ in a Barium crown glass,” Phys. Rev. Lett., 7, pp. 444 (1961)

[3] Etzel, H.W., Gandy, H.W., and Ginther, R.J., “Stimulated emission of infrared radiation from Ytterbium-activated silica glass,” Appl. Opt., 1, pp. 534 (1962)

[4] Poole, S.B., Payne, D.N., and Fermann, M.E., “Fabrication of low loss optical fibers containing rare earth ions”, Electron. Lett., 21, pp. 737 (1985)

[5] Mears W. J., “Neodymium-doped silica single mode fiber lasers”. Electron. Lett., 21, pp. 783 (1985)

[6] Kin, N.S., Hamada, T., Prabhu, M., Li, C., Song, J., Ueda, K, Liu, A., Kong, H.J., “Numerical Analysis and experimental results of output performance for Nd-doped double clad fiber lasers”, Opt. Commun., 180, pp. 329 (2000)

[7] Pask, H.M., Carman, R.J., Hanna, D.C., Tropper, A.C., Mackechnie, C.J., Barber, P.R, Dawes, J.M., “Ytterbium-doped silica fibre lasers: versatile sources for the 1-1.2 μm region”, IEEE J. Sel. Top. Quantum Electron., 1, pp. 2 (1995)

[8] Mundel, M., Engstrom, B., Kea, D., Laliberte, B., Minns, R., Robinson, R., “35-W single mode ytterbium fiber laser at 1.1μm”. Tech. Dig. CLEO’97. Postdeadline paper CPD30 (1997)

[9] Dominic, V., McCormack, S., Waarts, R., Sanders, S., Bicknese, S., “110W fiber laser” Electron. Lett., 35, pp. 1158 (1999)

[10] Jeong Y., Sahu, J.K., Baek, S., Alegria, C., Soh, D.B.S., Codemard, C., Nilsson, J., “Cladding-pumped ytterbium-doped large-core fiber laser with 610 W of output power” Opt. Commun., 234, pp. 315 (2004)

[11] Gapontsev, V., Gapontsev, D., Platonov, N., Shkurikhin, O., Fomin, V., Mashkin, A., Abramov, M., and Ferin, S., "2 kW CW ytterbium fiber laser with record diffraction-limited brightness " CLEO Europe, pp. 508 (2005)

[12] Weber, M.J., Lynch, J.E., Blackburn, D.H., and Cronin, D.J., "Dependence of the stimulated emission cross section of Yb3+ on host glass composition," IEEE J. Quantum Electron., QE-19, pp. 1600 (1983)

[13] Paschotta, R. Nilsson, J. Tropper, A.C. and Hanna, D.C. "Ytterbium-Doped Fiber Amplifiers" , IEEE J. Quantum Electron., QE-33, pp. 1049 (1997)

[14] Digonnet M., "Rare-earth doped fiber lasers and amplifiers", 2nd ed., Marcel-Decker, (2001)

[15] Desurvire, M., "Erbium-doped fiber amplifiers", Wiley-Interscience, (2002)

[16] Florea, C. and Winick, K. A. "Ytterbium-Doped Glass Waveguide laser Fabricated by Ion Exchange", J. Lightwave Technol., 1, pp. 1593 (1999)

Chapter II. Raman Fiber Laser

II.1. Introduction

Raman Fiber Lasers (RFL's) have become increasingly studied due to their effectiveness for wavelength conversion at wavelengths for which there is not conventional lasers available. RFL's that emit in the spectral region 1100-1700-nm are important in the development of various applications such as fiber optic communications, material processing, signal processing, laser spectroscopy and medicine [1, 2]. The principle of operation of a RFL is based on Stimulated Raman Scattering (SRS), a nonlinear optical process in optical fibers that changes the wavelength of a pump beam into another called stokes wave [3]. The Stokes wave itself serves as the pump for generating a second one, and so on. The Raman shift depends on the type of glass and quantity of impurities used in the process of manufacture. For example, the Raman shift in phosphor-silicate fibers is ~1330cm^{-1}, whereas this shift on germanium-silicate glass is ~440-cm^{-1} [4].

In this chapter we analyze the Raman gain spectrum of silica glass and situate the Stokes wave shifting when the fiber is pumped at certain wavelength. The background of SRS is also revised with emphasis on obtaining the Raman gain coefficient for any pump wavelength. Finally, we present the results of a RFL that contains a piece of Yb-doped fiber to decrease the operating threshold and increase the efficiency of the Stokes generated.

II.2 Raman Scattering

Raman Scattering is a nonlinear optical process that was first observed experimentally in 1928 by C.V. Raman [5]. Two types of Raman Scattering are of interest for its consequences in diverse fields: Spontaneous Raman Scattering (RS) and Stimulated Raman Scattering (SRS). Let us describe them right away.

II.2.1 Spontaneous Raman Scattering

An intense optical beam coupled to an optical fiber excites the molecules of the glass from the ground-state temperature-vibrating energy up to a virtual energy level (nonresonant state). From here, they decay instantaneously down to their initial energy passing through a higher-energy vibrating mode. In the process, from a quantum-mechanical viewpoint, each photon of energy ν_p produces two energy quanta: one Stokes photon of energy ν_s and one phonon. The Stokes photon coincides with the energy of an incident photon of the pump beam minus the energy of the phonon, being the later produced by the discrete transition from the higher-energy vibrating mode to the ground state, this is the spontaneous Raman scattering. Figure 1 shows a Stokes photon of energy $h\nu_s$ created spontaneously when an incident photon of energy $h\nu_p$ is excited up at a virtual level indicated as a dotted line. From a practical perspective, the incident beam coupled acts as a pump and generates the frequency-shifted radiation called Stokes wave [6].

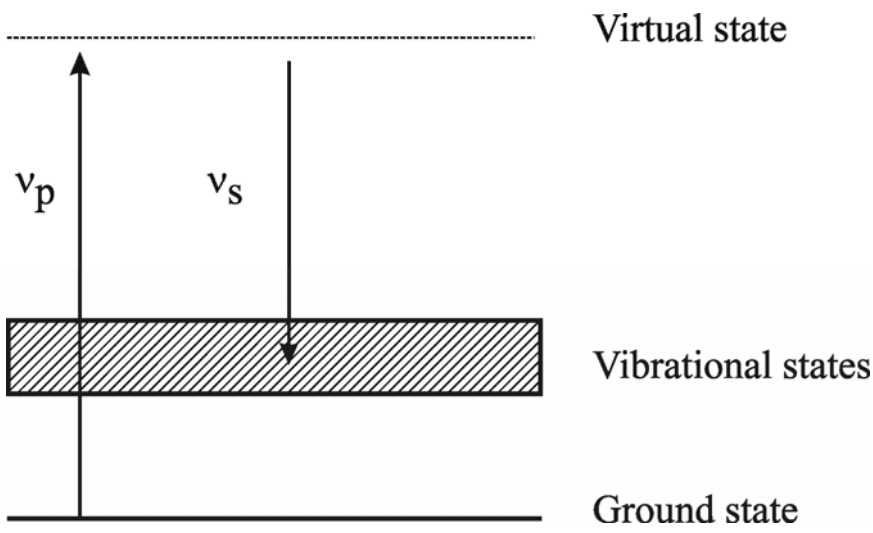

Figure 1. Energy levels diagram describing Spontaneous Raman scattering.

II.2.2 Stimulated Raman Scattering

The spontaneous Raman scattering generated in the fiber core uniformly radiates Stokes signal over all directions and the fraction that coincides with the numerical aperture (NA) of the fiber becomes guided along its axis in both the forward and backward directions. As this small signal ($<<10^{-4}$ fraction of the pump power) propagates, it attenuates by the background losses of the fiber material and at the same time (depending on the intensity of the pump power), amplifies by stimulating glass molecules to migrate from the virtual level down to the high-vibrating mode [6]. In this way, an avalanche process occurs and Stokes-signal amplification takes place. This is the stimulated version of the RS known as stimulated Raman scattering and it is the platform for the development of Raman fiber lasers and amplifiers [6, 7]. When increasing the pump power to a level at which the amplified Stokes signal becomes notorious at the output (i.e. the amplified signal overcomes the losses) the system reaches the threshold for Stokes generation.

II.2.2.1 Raman gain coefficient

Under the CW and quasi-CW regimes, the Stokes wave grows at a rate proportional to the pumping power described by [6]

$$\frac{dI_s}{dz} = g_R I_p I_s \tag{1}$$

where I_s is the Stokes intensity, I_p is the pumping intensity and g_R is the growth rate called Raman gain coefficient. The Raman gain only dependents on the wavelength of the pump given a certain material and its spectral shape depends on the overlapping of the discrete bands of the slightly different glass molecules as shown in Figure 2. The gain bandwidth covers over 40THz, with the dominant peak at ~13.2-THz, and g_R was normalized such that $g_R \approx 10^{-13}$-m/W at a pump wavelength λ_p=1000-nm, for other pump wavelengths Raman gain coefficient is obtained from the following relationship [8, 9]:

$$g_R(\lambda_p) = \left(\frac{1000\text{nm}}{\lambda_p}\right) 1.0\text{x}10^{-13}\ \text{m/W} \tag{2}$$

For example, if the pump is 1064-nm, then the Raman gain is $\approx 9.4\text{x}10^{-14}$ m/W and the peak value of the gain coefficient becomes centered at 1115-nm, this implies that 13.2-THz corresponds approximately to 50-nm.

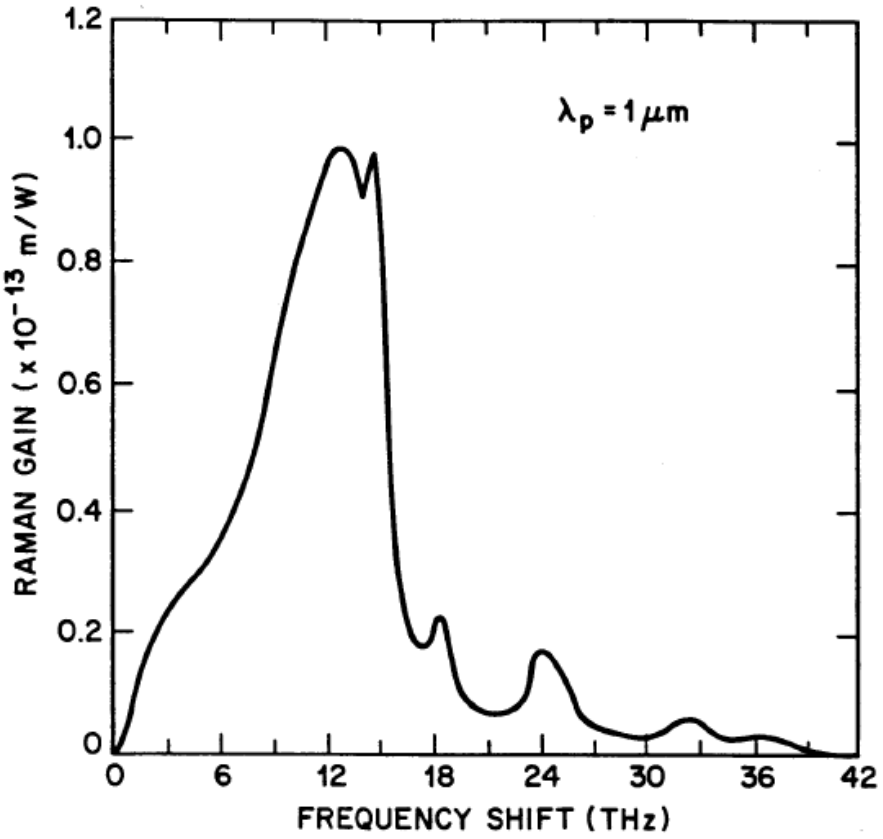

Figura 2. Raman gain spectrum in SiO_2 at pump wavelength 1000nm[10].

Again, if the pump is 1115-nm, then 13.2-THz corresponds to ~60-nm, this implies that the peak value of the gain coefficient is centered at 1175-nm. This natural shift is predicted by the next relationship [11],

$$\lambda_s = \lambda_p + \frac{\lambda_p^2}{c}\Delta\nu_s \tag{3}$$

where λ_p is the pump wavelength, λ_s is the peak value expected, and $\Delta\nu_s$ is the dominant peak considering a spectrum of Lorentzian shape, so that $\Delta\nu_s \approx 14\text{THz}$.

II.2.2.2 Raman threshold

The interaction between pumping and Stokes waves should be considered for calculation of the Raman threshold. In the CW case, the interaction of these waves propagating in the same direction is described by the following system of two coupled differential equations [6]:

$$\frac{dI_s}{dz} = g_R I_p I_s - \alpha_s I_s \tag{4}$$

$$\frac{dI_p}{dz} = -\frac{\nu_p}{\nu_s} g_R I_p I_s - \alpha_p I_p \tag{5}$$

where I_s is the Stokes intensity with a optical frequency ν_s, I_p is the pump intensity with optical frequency ν_p and g_R represents the material Raman gain coefficient, which scales inversely with the pump wavelength[6]. The absorption coefficients α_s and α_p account for the losses at the Stokes and pump frequencies, respectively.

Although pump depletion must be included for a complete description of SRS, it can be neglected for the purpose of estimating the Raman threshold. Equation (5) is readily solved if we neglected the first term on its right-hand side that is responsible for pump depletion. If we substitute the solution in Equation (4), we obtain

$$\frac{dI_s}{dz} = g_R I_P(0) \exp(-\alpha_p z) I_s - \alpha_s I_s \tag{6}$$

where $I_p(0)$ is the incident pump intensity at z=0. Equation (6) can be easily solved, and the result is

$$I_s(L) = I_s(0)\exp(g_R I_p(0) L_{eff} - \alpha_s L) \tag{7}$$

where L is the fiber length and

$$L_{eff} = \frac{1-\exp(-\alpha_p L)}{\alpha_p} \tag{8}$$

The solution (7) shows that, because of fiber losses, the effective fiber length is reduced from L to L_{eff}.

The use of Equation (7) requires an input intensity $I_s(0)$ at z=0. In practice, SRS builds up from spontaneous Raman scattering occurring throughout the fiber length. It has been shown that this process is equivalent to injecting one fictitious photon per mode at the input end of the fiber. Thus, we can calculate the Stokes power by considering amplification of each frequency component of energy $h\nu$ according to Equation (7) and then integrating over the whole range of the Raman-gain spectrum. The result is given by

$$P_s(L) = \int_{-\infty}^{\infty} h\nu \exp[g_R(\nu_p - \nu) I_p(0) L_{eff} - \alpha_s L] d\nu \tag{9}$$

This integral assumes that the fiber supports a single mode. Even though the functional form of $g_R(\Omega)$ is not known, the integral in Equation (9) can be evaluated approximately using the method of steepest descent because the main contribution to the integral comes from narrow region around the gain peak. Using $\nu=\nu_s$, we obtain

$$P_s(L) = P_{s0}^{eff}(z=0)\exp\left(g_R(\Omega) I_p(0) L_{eff} - \alpha_s L\right) \tag{10}$$

where the effective input power at z=0 is given by

$$P_{s0}^{eff}(z=0) = h\nu_s B_{eff}, \quad B_{eff} = \left(\frac{2\pi}{I_0 L_{eff}}\right)^{1/2} \left|\frac{\partial^2 g_R}{\partial \nu^2}\right|_{\nu=\nu_s}^{-1/2} \tag{11}$$

Physically, B_{eff} is the effective bandwidth of the Stokes radiation centered near the gain peak at $\Omega_R=\nu_p-\nu_s$. Although B_{eff} depends on the pump intensity and the fiber length, the spectral width of the dominant peak in Figure 2 provides an order-of-magnitude estimate for it.

The Raman threshold is defined as the input pump power at which the Stokes power becomes equal to the pump power at the fiber output [12] or

$$P_s(L) = P_p(L) = P_p(0)\exp\left(-\alpha_p L\right) \tag{12}$$

where $P_0(0)=I_0A_{eff}$ is the input pump power and A_{eff} is the effective core area. Using Equation (10) in Equation (12) and assuming $\alpha s \approx \alpha p$, the threshold condition becomes

$$P_{s0}^{eff}(z=0)\exp\left(g_R P_p(0) L_{eff} / A_{eff}\right) = P_p(0) \tag{13}$$

where P_{s0}^{eff} also depends on P_0 through Equation (11). The solution of Equation (13) provides the critical pump power required to reach the Raman threshold. Assuming a Lorentzian shape for Raman-gain spectrum, the critical pump power, to good approximation, is given by [12]

$$\frac{g_R P_0^{cr} L_{eff}}{A_{eff}} \approx 16 \tag{14}$$

A similar analysis can be carried out for backward SRS. The threshold condition in that case is still given by Equation (14) but numerical factor 16 is replaced with 20. As the

threshold for forward SRS is reached first at a given pump power, backward SRS is generally not observed in optical fibers. Of course, the Raman gain can be used to amplify a backward propagating signal. Note also that the derivation of Equation (14) assumes that the polarization of the pump and Stokes waves is maintained along the fiber. If the polarization is not preserved, the Raman threshold is increased by a factor whose value lies between 1 and 2. In particular, if the polarization is completely scrambled, it increases by a factor of two [6].

In spite of various approximations made in the derivation of Equation (14), it is able to predict the Raman threshold quite accurately. For example, 350-m HP-980 silica fiber at λp=1064-nm has optical losses of ~2.2-dB/Km, effective fiber length L_{eff}=320-m, effective area of A_{eff}=1.28x10^{-11}-m^2 and Raman gain coefficient of g_R=8.53x10^{-14}-m/W, the predicted Raman threshold is $P_0^{cr} \approx 7.5W$. Also assuming a Lorentzian gain profile with full width at half maximum $\Delta\nu$, the effective bandwidth, is given by [12]

$$B_{eff} = \frac{\sqrt{\pi}}{2} \frac{\Delta\nu}{(P_p(0) L_{eff} g_R / A_{eff})^{1/2}} \qquad (15)$$

Under these suppositions one can obtain an approximate value of the effective input power. If $P_p(0)$=7.5W, the effective input power is P_{s0}^{eff}=1.5x10^{-6}W. Figure 3 is a theoretical simulation using the Equations (4) and (5) that shows the Stokes wave evolution (dashed line) as consequence of the energy transfer of the pumping power (continuous line) inside 350-m HP fiber. One can observe that in the output end of the fiber the pumping power at z=350m is equal to the Stokes wave power when Raman threshold is $P_0^{cr} \approx 7.5W$.

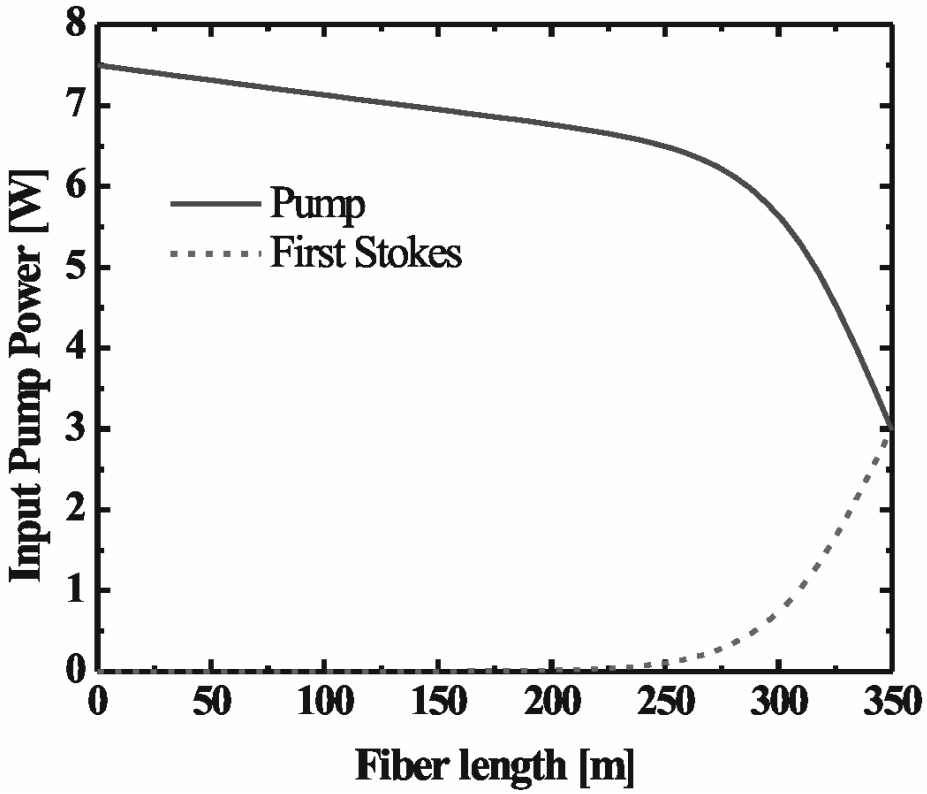

Figure 3 shows the propagation of the pumping power and the Stokes wave inside 350-m HP fiber.

In this thesis we call the power threshold for the Stokes generation the level of pumping power to which the amplified Stokes wave becomes notorious i.e. experimentally it is appreciated with our measurement systems. Figure 4 shows the fiber HP-980 pumped at 1064-nm in a free running configuration that consists of the pumping of the fiber cavity free of mirrors where the Stokes signal produced is fed back by 4% Fresnel reflection. At 4.429-W power threshold the Stokes wave power is ~ 200-mW.

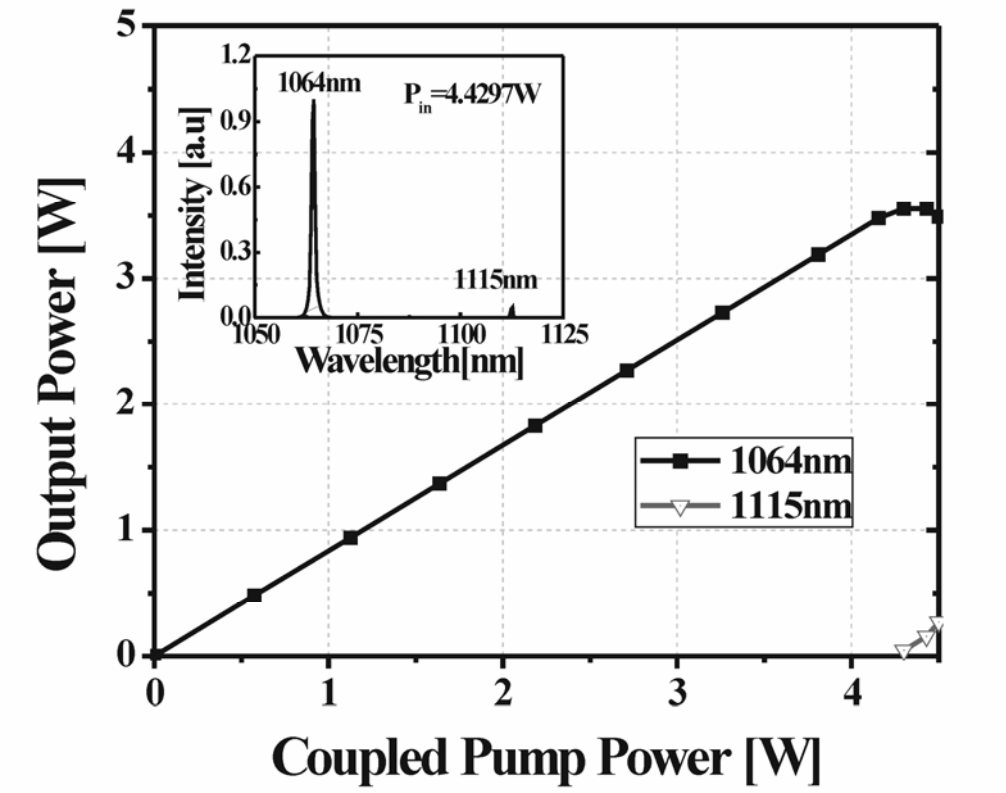

Figure 4. The squares and the triangles represent the evolution of the pump power and the signal Stokes, respectively.

In spite of that, a theoretical simulation at the same power threshold yields a value of the Stokes wave power of ~10-mW. The difference consists in that the theoretical simulation considers that the input pump power and the Stokes wave propagate in the same direction, while the experimental value is the result of the feedback of the Stokes wave due to the ~ 4% Fresnel reflection at the output end of the 980-HP silica fiber.

Once the power threshold is reached, the power is transferred from the pump to the Stokes. The theoretical simulation predicts a complete transfer of the pump power to the Stokes wave. In practice, however, the Stokes wave serves as a pump to generate a second-order Stokes wave if its power becomes large enough to satisfy Equation (14). This process of cascade SRS can generate multiple Stokes waves whose number depends on the input pump power [6].

In the following section we describe the Stokes waves in cascade when the feedback is higher than (>4%) the Fresnel reflection due to the use of Fiber Bragg Gratings (FBG).

II.3 Raman Fiber Lasers

In general a RFL consists of three elements: a pump source, a fiber (usually large) gain medium and a couple of FBG at the fiber ends [13]. A FBG results from a periodic perturbation of the refractive index in the core of an optical fiber which is realized by making use of the photosensitivity of certain types of optical fiber. In a FBG the incident optical field within the fiber is reflects by successive scattering from the index variations, i.e. it acts as a mirror that reflected a narrow range of wavelengths. Figure 5 shows the transmission spectrum for the FBG used in our experiments described in the chapter III.

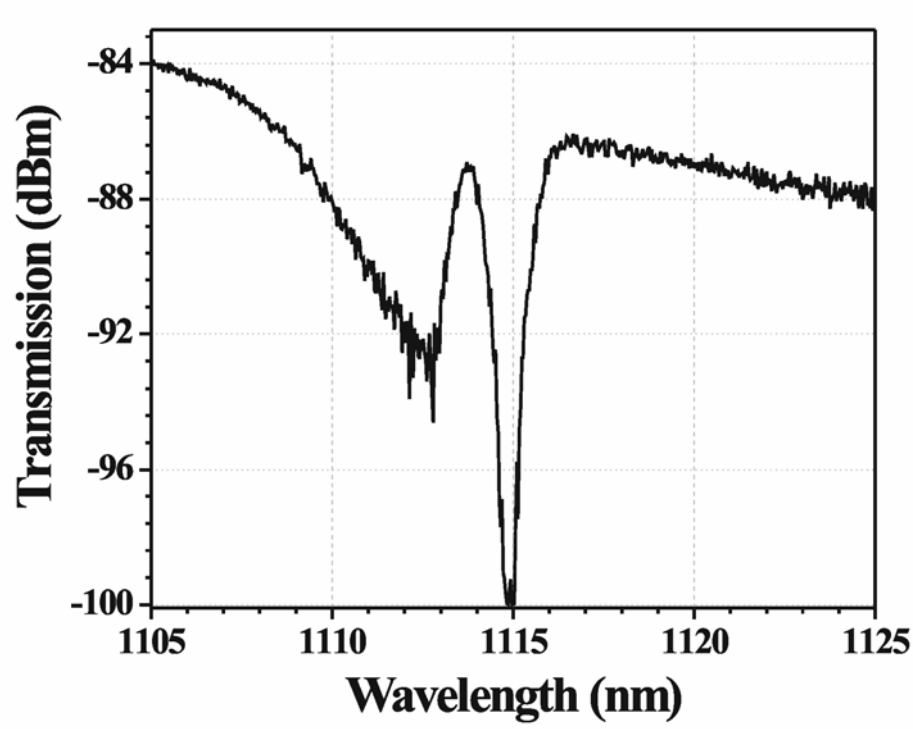

Figure 5 shows the transmission spectrum of the FBG centered at 1115nm.

The first reports of RFL's were based on a single cavity by the use of a couple of mirrors as Fabry-Perot resonator [14]. With the development of FBG's, it has been possible to have multiple cavities in a single fiber that are referred as cascaded Raman fiber lasers. Many reports using multi-cavities that generate Stokes signals in the range 1000 to 1700-nm have been published. Figure 3 illustrates the scheme of such configuration [15].

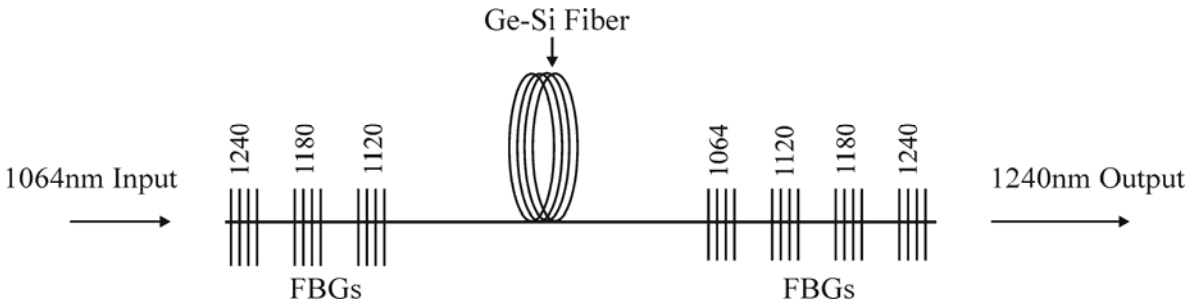

Figure 3. Linear configuration with fiber Bragg gratings nested.

In this configuration the pump beam at 1064nm is launched in a germanosilicate fiber and over 10^{-6} of this power is converted into spontaneous Raman scattering that co-propagates. This signal acts as a small Stokes wave that starts to grow as function of the distance traveled through the pumped length as described before. The 1064-FBG and 1120-FBG reflect the residual pump power and Stokes wave respectively. As the later reaches certain level, the 1120-nm radiation serves as the pump to generate another component that will eventually grow up and generate another one. The number of Stokes generated mainly depends on fiber length and pump power. Figure 4 depicts a representation of this multi-Stokes generation process.

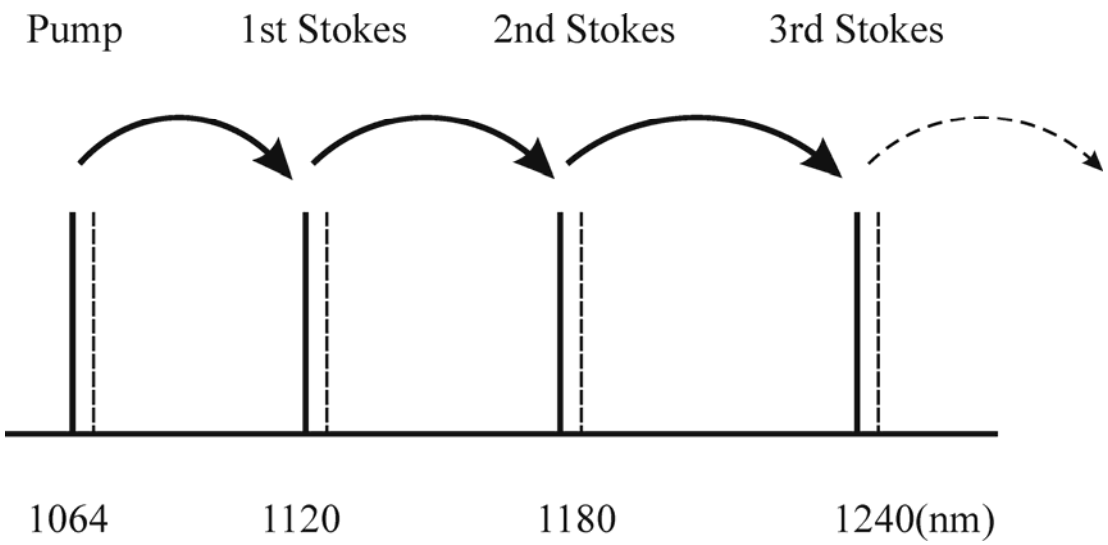

Figure 4. Cascaded multi-Stokes generation in a germanosilicate fiber. The solid vertical lines indicate the wavelength positions of the pump and the Stokes waves whereas the dotted lines show how the signal wavelength would change for wavelength changes of the pump [16].

The behavior of a RFL depends on parameters such as fiber length, FBG reflection, fiber losses, Raman gain coefficient and effective area. The evolution of the pump and the Stokes waves along the gain medium can be described by a set of nonlinear ordinary differential equations given by [13]

$$\frac{dP_p^{F/B}}{dz} = \mp\alpha_p P_p^{F/B} \mp \frac{g_R^1}{A_{eff}^1}\frac{\lambda_1}{\lambda_p}\left(P_1^F + P_1^B\right)P_p^{F/B} \tag{16}$$

$$\frac{dP_i^{F/B}}{dz} = \mp\alpha_i P_i^{F/B} \mp \frac{\lambda_{i+1}}{\lambda_i}\frac{g_R^i}{A_{eff}^i}\left(P_{i+1}^F + P_{i+1}^B\right)P_i^{F/B} \pm \frac{g_R^{i-1}}{A_{eff}^i}\left(P_{i-1}^F + P_{i-1}^B\right)P_i^{F/B} \tag{17}$$

$$\frac{dP_n^{F/B}}{dz} = \mp\alpha_n P_n^{F/B} \pm \frac{g_R^n}{A_{eff}^n}\left(P_{n-1}^F + P_{n-1}^B\right)P_n^{F/B} \tag{18}$$

Where the superscript F/B designates the forward and backward direction of travel of the waves, λ_i is the wavelength of the i-Stokes wave and n the lasing wavelength one. The first term on the right-hand side of each equation is the intrinsic fiber loss of the

corresponding wave: whereas the next term in Equation (17) describes their depletion by the forward and backward waves of the next highest Stokes. The third term in the Equation (17) and the second in Equation (18) represent the amplification of the ith and nth waves through Raman pumping by the (i-1)th and (n-1)th waves. The boundary conditions for these equations are given by

$$P_p^F(0) = P_{in} \qquad P_p^B(L) = R_p^b \cdot P_p^F$$
$$P_i^F(0) = R_i^f \cdot P_i^B(0) \qquad P_i^B(L) = R_i^b \cdot P_i^F$$
$$P_n^F(0) = R_n^f \cdot P_n^B(0) \qquad P_n^B(L) = R_{OC}^b \cdot P_n^F$$

Where R is the reflectivity of the front/back (f/b) Bragg grating, L is the length of the RFL cavity, and Roc is the reflectivity of the output coupler. For notational simplicity Pout=(1-Roc) $P_{out} = (1 - R_{oc})P_n^F(L)$ is used [13].

For a free running configuration (without FBG reflection) the pump and the signal in backward direction are not considerable, then, the Equations (16), (17) and (18) can be used to obtain numeric simulations for long silica fiber [9], where initial conditions for Stokes generation are given by the effective input power at z=0 (Equation (11)). The numeric simulation results are almost similar to the results obtained experimentally [15].

II.4 Conclusions

In summary, the Raman scattering is an inherent non lineal effect that characterizes optical fibers and it is detrimental in the telecommunication systems that operate at long distance. However, this phenomenon benefits other applications and under such conditions it is a powerful tool for generating new wavelengths that the conventional lasers do not emit. With the basic principles described in this and the first chapter, we realized the experiments that are described in the last chapter of this thesis.

References

[1] Kurkov, A S, Dianov, E M, Paramonov, V M, et. al., “High-power fibre Raman lasers emitting in the 1.22-1.34-μm range”, Quantum Electron., 30, pp.791 (2000)

[2] Zhao, Y, and Jackson, S. D., “Highly efficient free running cascaded Raman fiber laser that uses broadband pumping”, Opt. Express, 13, pp. 4731 (2005)

[3] Vanholsbeeck, F., Coen, S. and Emplit, P. “Cascaded Raman generation in optical fibers: influence of chromatic dispersion and Rayleigh backscattering”, Opt. Lett., 29, pp. 998 (2004)

[4] Huang, C., Cai, Z., Ye, C., Xu, H., Luo, Z., “Analytic modeling of the P-doped cascaded Raman fiber lasers”, Opt. Fiber Technol., 13, pp. 22 (2006)

[5] Headley, C, Agrawal, G P, “Raman amplification in fibre optical communication systems”, 3rd edition, Elsevier Academia Press, San Diego (2005)

[6] Agrawal, G. P. “Nonlinear Fiber Optics” 4th edition, Elsevier Academic Press, San Diego (2007)

[7] Bromake, J., “Raman Amplification for fiber Communications Systems”, IEEE J. Lightwave Technol., 22, pp. 78 (2004)

[8] Lin, C. Cohen, L.G. Stolen, R.H. Tasker, G.W. and French, W.G., "Near-infrared sources in the 1-1.3μm region by efficient stimulated Raman emission in glass fibers," Opt. Commun., 20, pp. 426 (1977)

[9] Murakami, Y, Noguchi, K, Ashiya, F., “Maximum measurable distances for a single-mode optical fibre fault locator using the stimulated Raman scattering (SRS) effect”, IEEE J. of Quantum Electron., 18, pp. 1461 (1982)

[10] Stolen, R. H., and Lee, C., “Development of the stimulated Raman spectrum in single-mode silica fibers”, J. Opt. Soc. Am. B., **1**, pp. 652 (1984)

[11] Shen Y. R., and Bloembergen, N., "Theory of stimulated Brillouin and Raman scattering," Phys. Rev., 137, pp. 1787 (1965)

[12] Smith, R. G. “Optical Power Handling Capacity of Low Loss Optical Fibers as Determined by Stimulated Raman and Brillouin Scattering”, Appl. Opt., 11, pp. 2489 (1972)

[13] Islam, M. N., “Raman Amplifiers for Telecommunications 2, Sub-Systems and Systems”, Springer, New York (2004)

[14] Auyeung J., and Yariv A., “Theory of cw Raman Oscillation in optical fibers”, J. Opt. Soc. Am., 69, pp. 803 (1979)

[15] Bertoni, A, “Analysis of the efficiency of a third order cascade Raman laser operating at the wavelength of 1.24μm”, Opt. Quantum Electron., 29, pp. 803 (1997)

[16] Rong, H., Xu, S., Cohen, O., Raday, O., Lee, M., Sih, V., and Paniccia, M., “A cascaded Silicon Raman Laser”, Nat. Photonics, 2, pp. 179 (2008)

Chapter III. RFL improvement by using Yb^{3+}-Doped Fiber

III.1. Introduction

Stimulated Raman Scattering (SRS) nowadays plays a major role in several applications such as fiber optic communications, material processing, pump sources, spectroscopy and medicine. SRS as the gain mechanism in optical fibers has been an effective way to amplify or shift signals into the 1000-1700-nm region [1, 2]. Lasers in the 1100-1200 nm are important to effectively pump Tm^{3+}-doped ZBLAN blue-emitting (upconversion) fiber lasers [3] and Ho^{3+}-doped ZBLAN ~3000-nm fiber lasers [4, 5]. Other applications of such lasers are frequency doubling to the 550-600-nm (green-yellow-orange) for medical purposes [6]. SRS technique is broadly explained in the chapter II.

In an optical fiber, the spontaneous Raman scattering (RS) uniformly radiates Stokes signal over all directions and the fraction that coincides with the numerical aperture (NA) of the fiber becomes guided along its axis in both, the forward and backward directions. As this small signal propagates, it attenuates by the background losses of the fiber material and at the same time (depending of the intensity of the pump power), amplifies by stimulating glass molecules to migrate from the virtual level down to the high-vibrating mode [7]. In this way, as in lasers, an avalanche process occurs and Stokes-signal amplification takes place. This is the stimulated version of the RS known as stimulated Raman scattering (SRS) and it is the platform for the development of Raman fiber lasers (RFL's) and amplifiers (RFA's) [7,8].

When increasing the pump power to a level at which the amplified Stokes signal becomes notorious at the output (i.e. the amplified signal overcomes the losses) the system reaches the threshold for Stokes generation. This is a free-running configuration with a relatively high threshold and poor conversion efficiency because only the forward propagating RS-signal amplifies and reaches the output. When placing a Stokes-wavelength high-reflectivity mirror at the pumping end, the forward signal reinforces and consequently, the conversion efficiency increases. This is usually realized by splicing fiber Bragg gratings (FBG's) to the amplifying fiber in a so-called "chained configuration". In this kind of configuration, the Stokes signals may reach powers comparable or superior to the pump [9].

An additional reinforcement, as we propose in this work, consists on splicing to the system a piece of Yb^{3+}-doped optical fiber placed between the FBG's and the un-doped fiber that produces in-axis amplified spontaneous emission (ASE) up to to ~1160 nm when pumped at 1064 nm [10,11]. The fact that ASE signal saturates at low powers in single mode fibers (tens of milliwatts absorbed) means that the doped fiber is practically transparent at high powers. Then, before the system reaches the non-linear operating conditions i.e. before producing the Stokes signal, the doped-fiber is providing its maximum ASE signal from which the FBG selects one spectral portion that serves as the "idle signal" to be amplified. In our work, an Yb^{3+}-doped fiber (YbDF) was inserted to a 1064-nm pumped RFL to lower the Stokes generation threshold. The initial threshold for first Stokes generation of ~2.9 W decreased to 1.9, 1.6 and 1.27 W when splicing respectively 34, 55 and 127 cm of Yb^{3+}-doped fiber; which means that the threshold decreased by 34, 45 and 56 % respectively. Then, at moderate pump powers at which the un-doped cavity did not produce stokes, the doped approach was producing first stokes at efficiencies ranging from 0 % at 1.25-W pump to 69 % at 2.9-W pump. As expected, the second Stokes signal at 1175 nm was also produced earlier in the doped configurations.

III.2. Experimental and results

The gain medium chosen for our experiments was a 980-HP silica fiber (fabricated by Nufern). White light was coupled to 1500-m of this fiber and the output spectrum (Power Vs Wavelength) was measured. Then, without de-coupling the white light, the last 1499-m were cut and a reference spectrum was obtained as well. The difference between these spectra gives the attenuation spectrum that corresponds to 1499-m of fiber. This is well known as the cut-back technique and the resulting spectrum in dB/km is shown in Figure 1.

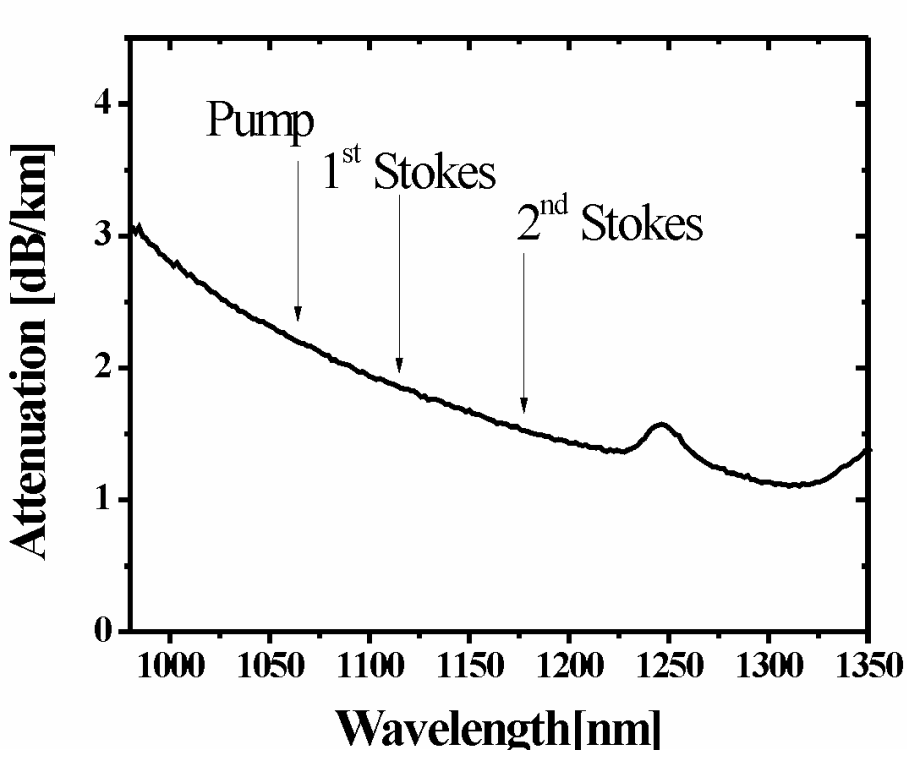

Figure 1. Spectral attenuation from 980 nm to 1350 nm yielding values of 2.2 dB/km, 1.86 dB/km and 1.6 dB/km at 1064 nm, 1115 nm and 1175nm, respectively for a 980-HP silica fiber.

Note that the optical losses at 1064, 1115 and 1175-nm in the 980-HP fiber were ~2.2, ~1.86 and ~1.6-dB/km, respectively. Then, the long fiber was pumped gradually by a 1064-nm fiber laser in a free-running configuration until we found the critical pump power for the Raman threshold, i.e., the power of first Stokes signal and the pump power obtained at the output end of the fiber were equal, the critical pump power (P_0^{cr}) was obtained at 2.46-W in 1055-m effective fiber length (L_{eff}) it allowed us to estimate the Raman gain efficiency (g_R/A_{eff}) with the Equation (14) described in chapter II to be 6.16-$km^{-1}W^{-1}$. These parameters introduced in standard equations described in section II.2.2.2 of chapter II gave us the required fiber length to reach the power threshold for generating (weak) first-Stokes signal at coupled powers around 4.5-W.

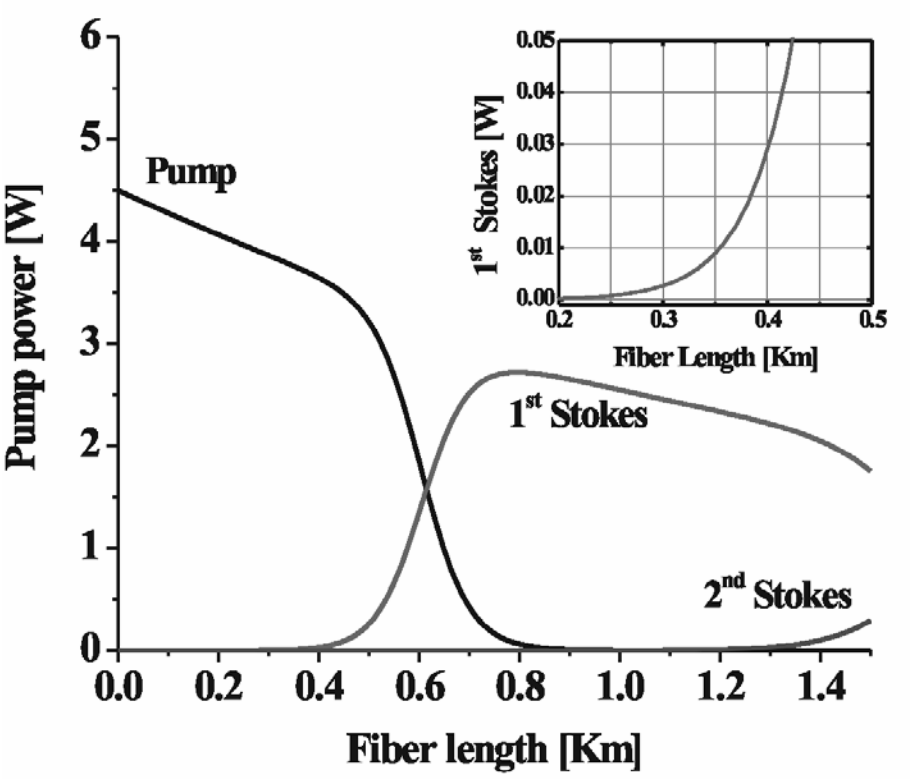

Figure 2. Pump power evolution and 1st and 2nd Stokes wave at 4.5-W coupled pump power. The inset is an amplification corresponding from 0.2 to 0.5-Km of fiber length.

Although the limit of operation of coupled power of the pumping system was 9W, in our numeric simulation we choose 4.5W of power coupled to have a margin of operation of 50% in our experiments, and a fiber length of 1499-m. We choose 10mW as the Stokes power minimum observable with our mensurement systems, and where the attenuation of the coupled pump power at the output is for up of 80%. The inset in Figure 2 shows that 10-mW Stokes power corresponds at 350-m HP fiber.

In this way, 350-m was the chosen length of the 980-HP fiber to use in three configurations: (a) free-running, (b) chained, and (c) chained with a spliced 10000-ppm YbDF (chained-ASE configuration). A scheme of the most complete configuration is shown in Figure 3.

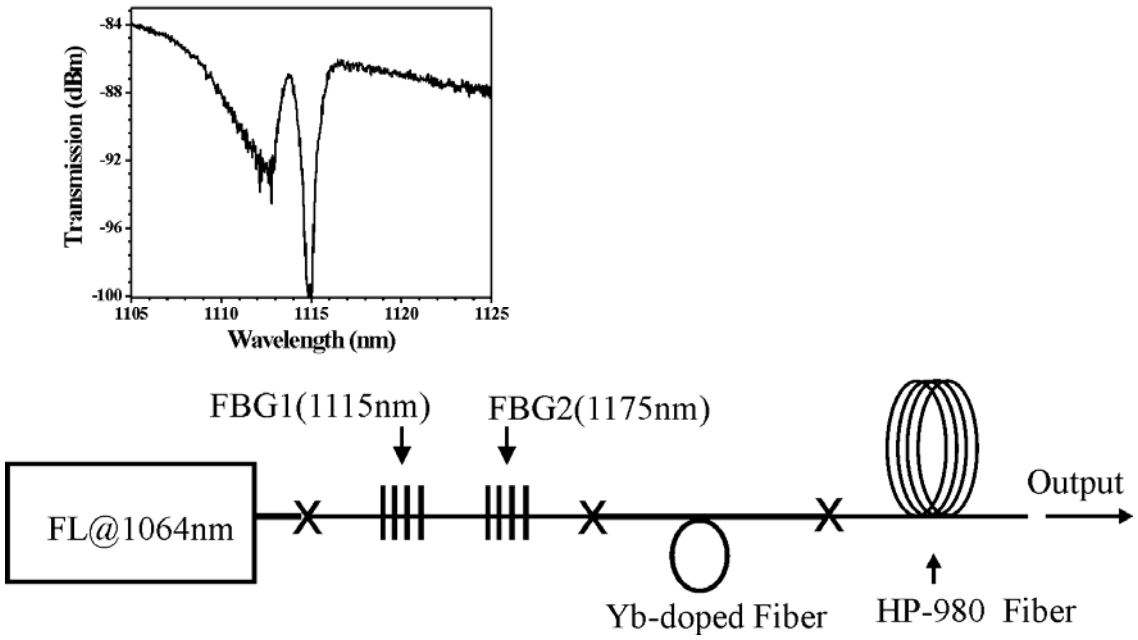

Figure 3 Scheme of the chained-ASE experimental configuration. The inset shows the transmission spectrum of FBG1.

In all configurations, the output end of the fiber was flat (~ 4 % reflection). The FBG's were patterned on Flexcor-1060 SM fiber with core diameter of ~6 μm. The transmission spectrum of the one coinciding with the first Stokes signal is shown in the

inset of the figure; the other one was not characterized because the ASE signal at 1175 nm was practically zero. Note that the main reflecting peak of FBG1 (1115 nm with a bandwidth ~1.3 nm) coincides with the first Stokes signal that corresponds to a 13.2 THz shift in silica fiber [7]. The YbDF and the 980-HP fiber have the same core diameter, 4.2 μm. An optically isolated CW 1064-nm fiber laser was spliced to each configuration with splicing losses of 0.45 dB to the FBG's and 1.8-dB to the 980-HP fiber. The measured coupling efficiency from the FBG to the YbDF was ~ 64 % and from the YbDF to the 980-HP was close to 100 %. Then, the corresponding compensations were realized in order to account for coupled power in the 980-HP fiber.

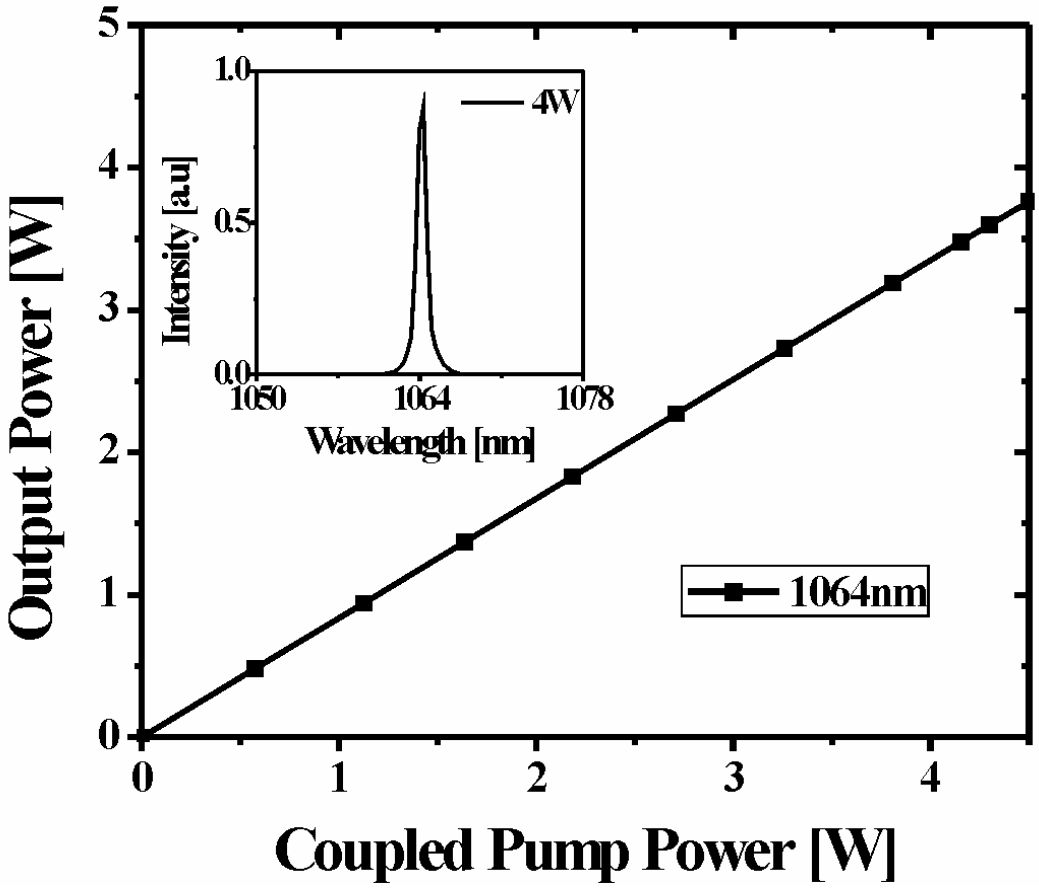

Figure 4 Output power as a function of coupled pump power in the free running configuration. The inset shows the output spectrum at 4 W of pump power.

In the free running configuration, the 350-m silica fiber alone was used as the Raman gain medium and the Figure 4 shows the output power versus the pump power (see the spectrum in the inset). The first stokes (not shown in figure) just appeared at ~4.5 W. The difference between the output power and the coupled power corresponds to the propagation losses of the 980-HP fiber, ~2.2-dB/km, which is in close agreement with Figure 1.

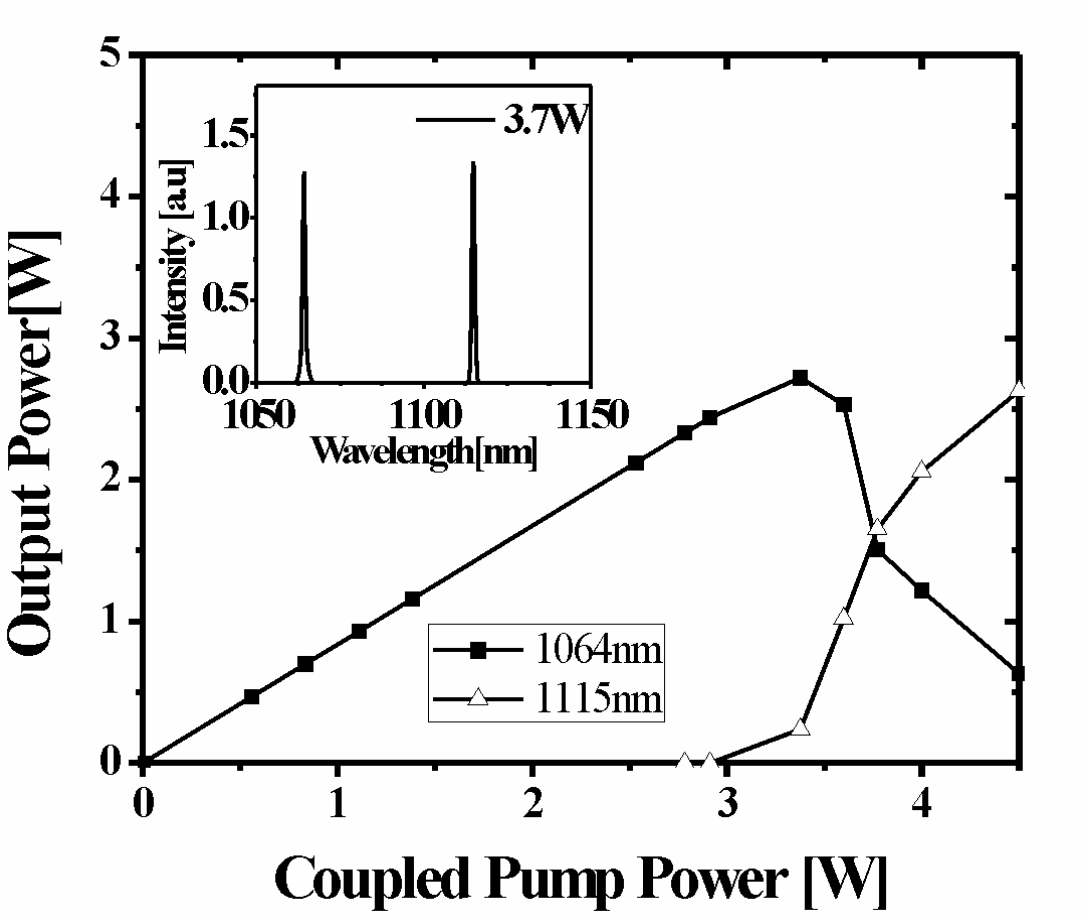

Figure 5. Output power versus coupled pump power in chained configuration. The inset shows the output spectrum at 3.7 W of pump power.

Next, we implemented the chained configuration and obtained the result of Figure 5. In this case, the first stokes-generation threshold was ~ 2.9-W. As a reference, the conversion efficiency at 4-W was ~52%. The curves composed of squares and triangles represent respectively, the residual pump and the first Stokes delivered, whereas the inset shows the spectrum at 3.7-W-pump (each signal was 1.6-W). The bandwidths are 0.9 (pump) and 0.88-nm (1st stokes). Power delivered at each signal was estimated as the quotient of the area under the curve of its spectral profile over the area corresponding to the full spectrum. Up to this point, except for the type of fiber used, nothing is new; the system behaves as expected in a chained configuration.

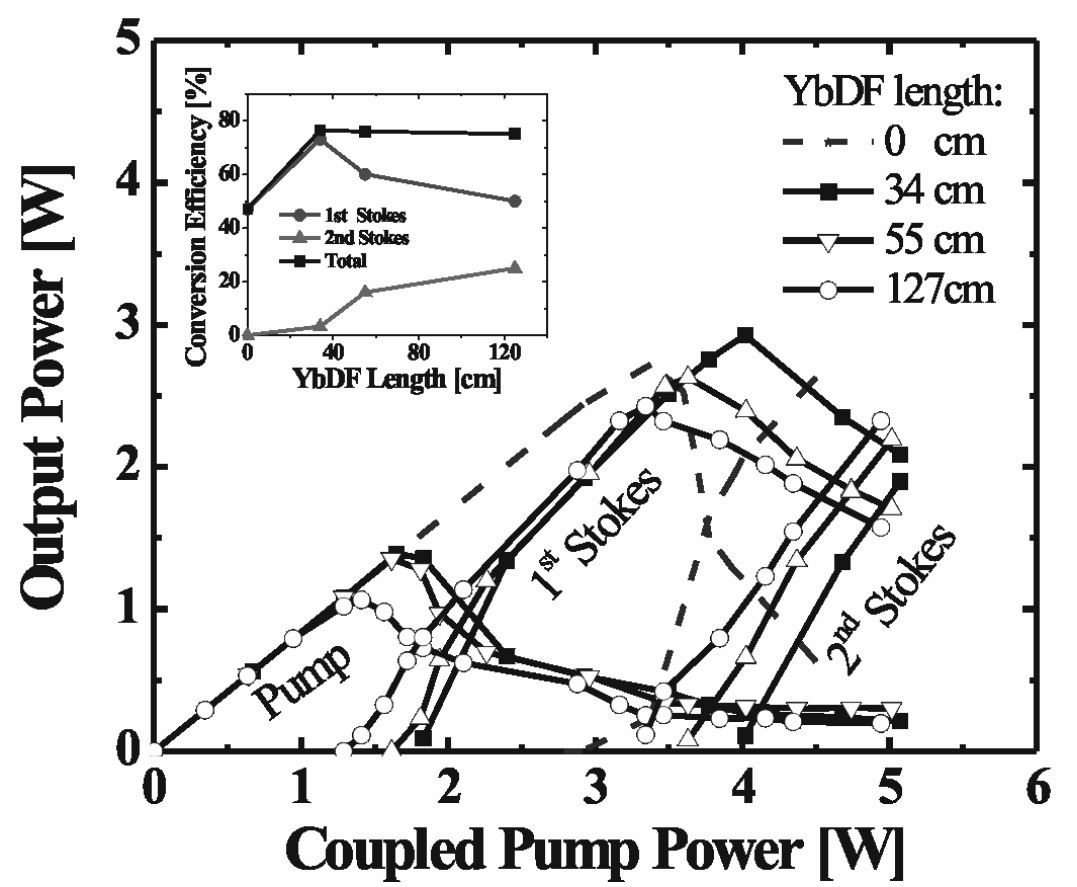

Figure 6. Output power as a function of coupled pump power for the chained-ASE configuration. The inset shows the total conversion efficiency and the corresponding to each stokes signal as function of YbDF length.

Our major contribution consists on a noticeable improvement when three pieces of 10000 Yb^{3+}-doped fiber were spliced between the FBG's section and the test fiber (as depicted before in Figure 1). The data from measurements are plotted in Figure 6 and the dotted curve is the same of Figure 4, it was used as a reference because it corresponds to 0-cm of doped-fiber. Curves composed of squares, triangles and circles correspond respectively to 34, 55 and 127-cm of Yb^{3+}-doped fiber.

Note that there is a notorious difference between the un-doped and the doped cavities. By defining the threshold for Stokes generation as the intersection of the curves with the horizontal axis, the initial 2.9-W threshold for 0 cm decreased to 1.9 W for 34 cm, 1.6 for 55 and 1.27 for 127-m, representing threshold enhancements of 34, 45 and 56 %. Hence, the improvement depends on doped fiber length. As expected, the second stokes signal, only present with this approach, was also dependent on doped-fiber length. The inset contains the optical conversion efficiencies for the stokes-signals as a function of YbDF-length at 4-W pump power. Although the conditions are different at different pump powers, note that at 4-W, 34-cm of YbDF were optimal to have the highest efficiency (75%) of 1115-nm with the lowest residual power (6.25%). Regarding the second stokes, we attribute its earlier generation as a consequence of Raman Scattering produced by the first stokes more than ASE from the YbDF because: a) the latter produced very weak signal at 1175-nm and b) the SRS process starts at any point along the cavity i.e. not necessarily close to the YbDF or FBG. In all the chained-ASE configurations the residual pump saturated to ~0.25 W (6.25%) for powers $\geq$ 4W. In order to extrapolate the results, we plotted the pump power threshold (P_{th}) versus YbDF-length (L) and fitted the data points to a exponential function of the form $P_{th} = 1.248+1.6525 \cdot Exp(-L/36.1)$ [see Figure 7]. Then, the minimum threshold for very large fibers would be 1.248 W which seems very close (22-mW) to the value obtained with the longer fiber, 1.27-W for 127-centimeters.

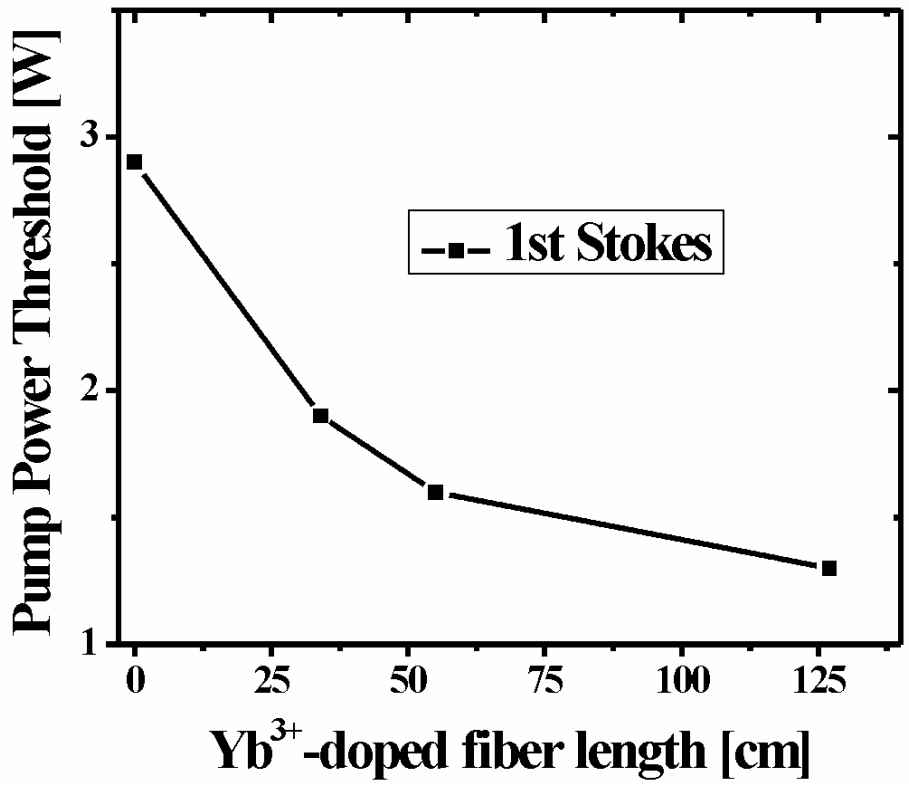

Figure 7. Pump power threshold for first stokes generation as a function of YbDF length.

Based on these results, we believe that having the dopants distributed along the entire Raman gain medium might improve the approach because adverse effects related to high concentration (such as quenching) would be reduced and the second stokes generation would be enhanced as well. An additional enhancement for the second stokes generation is possible by heating the fiber some tens of degrees Celsius as reported in Ref [6] where the ASE emission was IR-shifted. Two additional stokes (up to 1310-nm) are easily generated by increasing the fiber length by some hundreds of meters and two FBG's. The fact that ASE saturates at low power makes it possible to use co-dopants activated by the fundamental or stokes signals to enhance Raman-generated signals at other regions.

However, for covering the zero dispersion region of silica fibers, the interval beyond 1300-nm, there is not a rare-earth doped silica-fiber that may enhance the signals. Then, it would be advisable to go directly by using a single phosphosilicate-fiber pumped between the first and second Stokes to generate signals in the 1292-1350 nm interval [12].

III.2. Discussions

A.S. Kurkov et. al [6] obtained laser emission at 1160-nm with a lasing efficiency slope of 45%. The gain consisted on 50-m of YbDF heated up to 70ºC and pumped into the core with another Yb-laser that emitted at 1070-nm and the cavity was formed by 1160-nm FBG's. By contrast, we used short pieces of YbDF inside a resonant cavity formed by 350-m of silica fiber and two BG's that operated at 1117 and 1175-nm. When was coupled 4-W pump power and 34-cm YbDF inside our laser scheme we obtained the highest conversion efficiency (75%) in 1117-nm Stokes wave. When the YbDF length was 127-cm we obtained an output power of 74% distributed between 1117-nm (~50%) and 1175-nm (~24%) Stokes waves.

The advantages of our experimental configuration were: very short YbDF length, no external devices that heated the YbDF, the resonant cavity for each Stokes was formed by a fiber BG and the ~ 4% Fresnel reflection at the end of the silica fiber ensuring efficient output power. These advantages make our experimental configuration very versatile and cheap in comparison of that used by A.S. Kurkov et. al.

III.3. Conclusions

The amplified spontaneous emission produced by some rare earths as dopants in silica fibers may play an important role for improving Raman converters as reported here for Yb^{3+}. By splicing a short piece of doped fiber inside a Raman converter, it was possible to decrease its power threshold for the Stokes generation and as a consequence, to increase the conversion efficiency, in the first and the second Stokes.

The amplified spontaneous emission at 1064-nm pump power produced for the shortest YbDF length is centered on wavelengths next to the pump power, while in the longest YbDF length the amplified spontaneous emission is centered on wavelengths very distant to the pumping power.

The conversion efficiency to first Stokes was better for the shortest YbDF length (34cm), while the long YbDF length exhibited high conversion efficiency to second Stokes (127cm).

The cost per pumping watt and the high loss to overcome in long fibers are the most important issues to consider in the design of fiber Raman converters. The scheme presented here may contribute to reduce the cost of these systems because short pieces of doped fiber (as the ones used here) do not cost more than tens of dollars at present. We believe that this approach, as others discussed in this work, will contribute to reduce the cost of these systems.

To future we seek to improve the second Stokes by carrying out the following modifications: to increase the reflectivity in the output end of the silica fiber splicing a BG fiber operating at 1115-nm to a higher value than 4%, to increase the YbDF length, to increase the silica fiber length, to demonstrate the mechanism for other optical fibers (LEAF, SMF-28, true wave, etc.) and with other RE-doped fiber.

References

[1] Dianov, E.M. and Prokhorov, A.M., "Medium-power CW Raman fiber lasers", IEEE J. Select. Top. Quantum Electron., 6, pp. 1022 (2000)

[2] Zhao Y. and Jackson, S., "Highly efficient free running cascaded Raman fiber laser that uses broadband pumping", Opt. Express, 13, pp. 4731 (2005)

[3] Talavera, D.V. and Mejia, E.B. "Blue up conversion Tm3+ doped fiber laser pumped by a multiline Raman source", J. Appl. Phys., 97, pp. 053103 (2005)

[4] Talavera, D.V. and Mejia, E.B., "Holmium –doped fluoride fiber laser at 2950nm pumped at 1175nm", Laser Phys. 16, pp. 436 (2006)

[5] Librantz, A.F.H., Jackson, S.D., Gomes, L., Ribeiro, S.J.L. and Messaddeq, Y. "Pump excite state absorption in holmium –doped fluoride", J. Appl. Phys., 103, pp. 023105 (2008)

[6] A.S. Kurkov, V.M. Paramonov, and O.I. Medvedkov, "Ytterbium fiber laser emitting at 1160nm" Laser Phys. Lett. 3, pp. 503 (2006)

[7] G. P. Agrawal, "Nonlinear Fiber Optics", 3rd edition, Academic Press, San Diego, CA (2007)

[8] Bromake, J., "Raman amplification for fiber communications systems", IEEE J. Lightwave Technol. 22, pp. 78 (2004)

[9] Bertoni, A. "Analysis of the efficiency of third order cascaded Raman laser operating at the wavelength of 1.24μm", Opt. Quantum Electron., 29, pp. 1047 (1997)

[10] Pask, H.M., Carman R.J., Hanna D.C., Tropper A.C., Mackechnie C.J., Barber P.R, Dawes J.M, "Ytterbium-doped silica fibre lasers: versatile sources for the 1-1.2 μm region", IEEE J. Select. Top. Quantum Electron., 1, pp. 2 (1995)

[11] Coïc, H., "Analytical modeling of high gain ytterbium-doped fibre amplifiers", J. Opt. A: Pure Appl. Opt. 4, pp. 120 (2002)

[12] Kurkov, A.S., Dvoyrin, V.V., Paramonov, V.M., Medvedkov O.I., and Dianov, E.M., "Ytterbium fiber laser emitting at 1160 nm" Laser Phys. Lett. 4, pp. 449 (2007)

Appendix 1

List of Publications

L. de la Cruz-May, J. A. Álvarez-Chávez, A. Martínez-Ríos, I. Torres-Gomez and A. Flores-Gil "Critical Pump Power and Cross-Section Calculation for Yb^{3+}-Doped Novel Inner-Clad Structures" Laser Physics, 3, 18, 349-352, (2007)

F. Martínez-Piñon, J. A. Alvarez-Chavez, L. de la Cruz-May, And G. Martinez-Romero, "Optimum Peak pulse Investigation for OTDR Instrumentation", Laser Physics, 7, 18, 907-910 (2007)

F. Martínez-Piñon, J. A. Alvarez-Chavez, D. Jaramillo-Vigueras, L. de la Cruz-May, And H. L. Offerhaus, "Linear Polarization Yb3+-Doped Fiber Laser with Novel Inner clad Structures", Laser Physics, 11, 18, 1340-1343 (2008)

L. de la Cruz-May, and E. B. Mejia, "Raman Fiber Laser Improvement By Using Yb3+ Doped Fiber", Laser Physics, 5, 19, 1017-1020 (2009)

L. de la Cruz-May, J.A. Álvarez-Chávez, A. Martínez-Ríos, I Torres-Gómez, A. Torres-García, A. Flores-Gil. "Linear-polarization Yb^{3+} -doped fiber laser with novel inner clad structure", Multiconference on Electronics and Photonics, Guanajuato Mex. (2006)

J.A. Álvarez-Chávez, L. de la Cruz-May, A. Martínez-Ríos, I Torres-Gómez, F. Martínez-Piñón. "High power Er3+/Yb3+ doped fiber laser suitable for medical applications", Multiconference on Electronics and Photonics, Guanajuato Mex. (2006)

L. de la Cruz-May, E. Mejía-Beltrán, J. A. Álvarez-Chávez "Experimental and theoretical nth-order Cascaded Raman Fiber Laser Generation using a Large Effective Area Fibre", Encuentro de Investigación en Ingeniería Eléctrica. Zacatecas, Mex. (2008)

J. A. Álvarez-Chávez, L. de la Cruz-May, F. Martínez-Piñón, E. Mejía-Beltrán, C. Carrillo-Delgado, G. Martínez-Romero, "1.1.3um Double Clad, Rare-Earth-doped Fibre Laser Sources: Critical Power Simulation", Encuentro de Investigación en Ingeniería Eléctrica. Zacatecas, Mex. (2008)